Electrochemical Study of Ionic Liquids Aiming at Development of In Situ Electron Microscope Technologies

（電子顕微鏡その場観測技術の開発を目的としたイオン液体の電気化学的研究）

2009

SATOSHI ARIMOTO

Department of Applied Chemistry

Graduate School of Engineering

Osaka University

Department of Applied Chemistry

Graduate School of Engineering

Osaka University

Yamada-oka 2-1, Suita, Osaka 565-0871, Japan

March, 2009

Preface

The studies presented in this thesis were carried out under the guidance of Professor Dr. Susumu Kuwabata at Department of Applied Chemistry, Graduate School of Engineering, Osaka University.

The objectives of this thesis are elucidation of the unknown characteristic features of ionic liquids and development of their new applications. Ionic liquids have been attracting much interest from the view point of not only industrial electrochemistry but also various chemical fields. The author hopes sincerely that the knowledge obtained in this work would contribute to progress in the field of electrochemistry and vacuum technologies such as electron microscopes.

A part of chapter 1 was conducted in collaboration with Professor Dr. Charles L. Hussey at Department of Chemistry and Biochemistry, The University of Mississippi, USA.

Satoshi Arimoto

Contents

General Introduction

Background

Ionic liquids, which are room temperature molten salts, have been receiving considerable attention because they have some specific properties such as non-volatility, low-combustibility, ionic conductivity and ability to dissolve many kinds of substances. In the electrochemical field, it would be one of the most notable features that ionic liquids possess considerably wide potential window, since they consist of cation and anion and behave as an electrolyte without any solvent.[1-18] In case of aqueous solution, for example, effective potential range is restricted by electrolysis of solvent (water) and/or supporting electrolyte. Therefore, ionic liquids have been expected to show their inherent electrochemical behaviors which cannot be seen in conventional aqueous and non-aqueous solutions. However, their properties as electrolyte have not yet been completely elucidated because electrochemical theories for electrolyte without any solvent are not yet established.

Investigation of ionic liquids including molten salts was commenced from 1950s in relation with aluminum industry. In the initial research using $AlCl_3$-base ionic liquid by F. H. Hurley and T. P. Wier, eutectic point was reduced to as low as –40 °C for hygroscopic 66.7-33.3 mol% $AlCl_3$–ethylpyridinium bromide.[19] Since the first water- and air-stable ionic liquid of 1-ethyl-3-methylimidazolium tetrafluoroborate was reported by J. S. Wilkes and M. J. Zaworotko in 1992,[20] not only electrochemists but also scientists in various fields have been interested in the novel salts,[21-30] based on the fact that many kinds of ionic liquids could be designed easily by changing the combination of cation and anion.

Electron microscopes, such as scanning electron microscope (SEM) and transmission electron microscope (TEM) give magnified still images and elemental information with energy dispersive X-ray fluorescence (EDX) analysis. However, since electron microscope observation is conduced under vacuum condition, it has been impossible to introduce any liquid into the vacuum chamber so far. Even if a low-vacuum SEM is used, a wet sample like water-containing biomaterial must be frozen. Furthermore, it is necessary for insulating samples to be subjected to multistep pretreatments such as coating of metal and carbon by vapor deposition or sputtering under vacuum condition in order to avoid charging of the sample during observation.

It was recently reported that very slow vaporization of some ionic liquids is detected under severe condition; high vacuum and high temperature.[31] In other words, it was confirmed that no analysis conducted under high vacuum conditions can detect the vaporization of ionic liquids at room temperature.[32, 33] This has encouraged the introduction of ionic liquids into several vacuum techniques including SEM,[34] TEM,[35, 36] XPS[37-41] and SIMS,[41, 42] remaining their fluidity. If it were possible to observe chemical phenomena with electron microscopes and EDX in real time, this would be a powerful tool for clarification of reaction mechanisms.

The Present Work

The present study has been conducted focusing on utilization of ionic liquids as solventless electrolyte solutions and antistatic agents of insulating materials for electron microscopes. Based on these findings, it was then attempted to develop a new technique of in situ SEM observation of electrochemical reactions in ionic liquids. This thesis consists of four chapters.

Chapter 1 deals with electrochemical reaction using ionic liquids as electrolyte solutions. As an example, electrochemical reductive desorption of *n*-alkanethiol self-assembled monolayer (SAM) was chosen. This reaction is well known to be strongly affected by electrolyte and solvent. Another electrochemical reaction chosen was electrodeposition of aluminum alloys from $AlCl_3$–1-ethyl-3-methylimidazolium chloride, as the particular reaction which cannot be conducted in aqueous solution. Chapter 2 introduces the application of ionic liquids to the antistatic agents for electron microscopy. Considering living specimen including water, the use of ionic liquids must give desired methods to observe true features of the samples with electron microscopes. Chapter 3 concerns development of in situ electrochemical SEM technique using ionic liquids as electrolyte solutions. Redox reaction of conducting polymer which accompanies volume changes is adopted. At the same time, in situ EDX analysis is also attempted. In chapter 4, electrodeposition of silver is observed with SEM in real time. Here, the deposition processes are compared with the predicted morphologies from the electrochemical behaviors.

Chapter 1

Evaluation of Electrochemical Reaction Using Ionic Liquids as Electrolyte Solution

1-1. Introduction

Since ionic liquids consist of only ionic species without solvent, they have been expected to show specific electrochemical behaviors which cannot be interpreted by the conventional theories. Therefore, it is required to consider if ionic liquids could be utilized as electrolyte solution. For this purpose, electrochemical reductive desorption of *n*-alkanethiol self-assembled monolayer (SAM) and electrodeposition of aluminum alloy in ionic liquid have been investigated.

Since the first report by Allara and Nuzzo in 1983,[43] *n*-alkanethiol SAM formed on a metal substrate (Au, Pt, or Cu) has been intensively studied. The SAM possesses highly organized structure developed by van der Waals forces between alkyl chains. However, as reported first by Porter et al.,[44] the closely packed monolayer can easily be desorbed by electrochemical reduction formulated by

$$\text{R-S-M} + e^- \rightarrow \text{R-S}^- + \text{M} \qquad (1)$$

where R and M represent an alkyl chain and a metal electrode, respectively. This reaction is sensitive to several parameters, including length of the alkyl chain, kind of electrolyte solution, and kind of metal substrate.[44-74] Then it was attempted to investigate of ionic liquids focusing on roles of cations and anions in this reaction.

On the other hand, Lewis acidic ionic liquids, such as aluminum chloride–1-ethyl-3-methylimidazolium chloride have been investigated focusing on electrodeposition of aluminum-transition metal alloys.[75-81] These alloys are deposited from solutions containing dissolved low–valent transition metal ions, which are reduced at potentials equal to or slightly negative of that for the electrodeposition of Al in these ionic solvents. It is impossible to conduct these reactions in aqueous solution due to electrolysis of water. Moreover, aluminum-transition metal alloys exhibit enhanced resistance to chloride–induced corrosion relative to pure Al.[78-83] The purpose of this work is preparation and evaluation of ternary Al-Mo-Ti alloy.

1-2. Experimental

1-2-1. Preparation and electrochemical desorption of alkanethiol SAM

An Au/mica electrode substrate having a quasi (111) surface was prepared by vacuum evaporation of Au on a freshly cleaved natural mica sheet (Nilaco Co.) heated at 290 °C. The electrode coated with the SAM of four kinds of *n*-alkanethiols, *n*-propanethiol, *n*-hexanethiol, *n*-octanethiol and *n*-decanethiol (Wako Pure Chemical Ind.), was prepared by immersing the Au/mica substrate in 1 mM alkanethiol/ethanol for 3 h at room temperature. Their alkyl chain lengths will be indicated in this thesis by numbers of carbon atoms (n of $C_nH_{2n+1}SH$).

The electrochemical cell used was a Pyrex glass tube (ϕ1.5 cm × 9 cm), both ends of which were open. The SAM coated electrode was placed at the bottom hole of the cell with a silicone rubber O-ring (apparent electrode area of 0.36 cm^2), and the top hole was tightly fitted with a silicon rubber stopper having a Pt foil counter and Ag/Ag^+

(0.1 M) reference electrodes.[84-87] The effective surface area of the electrode, which was determined from the electric charges of anodic oxidation of chemically adsorbed iodine,[88] was 0.40 cm^2. Linear sweep voltammetry was conducted using a potentiostat (Hokuto Denko, HSV-100) in a dry-argon atmosphere glove box (Miwa Co., Ltd., 1ADB-3). Ionic liquids used for this measurements, 1-ethyl-3-methylimidazolium tetrafluoroborate (EMI-BF_4), 1-butyl-3-methylimidazolium tetrafluoroborate (BMI-BF_4), 1-ethyl-3-methylimidazolium bis(trifluoromethanesulfonyl)amide (EMI-TFSA) and 1-butyl-3-methylimidazolium bis(trifluoromethanesulfonyl)amide (BMI-TFSA) were purchased from Kanto Chemical Co., Inc. and were dried under vacuum at 105 °C for 3 h at least prior to use.

Computational simulation of linear sweep voltammograms was carried out using a program that was composed by Visual Basic 6.0 based on a formula considering the stabilizing energies due to thiol-thiol and thiol-solvent interactions.[44-54, 89]

1-2-2. Preparation and characterization of electrodeposits

The procedures used for the synthesis and purification of EMI-Cl, the sublimation of $AlCl_3$, and the preparation of a Lewis acidic 66.7-33.3 mol% $AlCl_3$–EMI-Cl ionic liquid were identical to those described in other reports.[76] Solutions of Mo(II) and Ti(II) in the $AlCl_3$–EMI-Cl were prepared by the addition of anhydrous molybdenum(II) chloride, $(Mo_6Cl_8)Cl_4$ (Cerac) and anhydrous titanium(II) chloride (Aldrich), respectively. After preparing stock solutions of Mo(II) and Ti(II), the composition of each plating bath was adjusted by combining these stock solutions as needed. All experiments were conducted in a nitrogen gas-filled glove box (Vacuum Atmospheres Co. NEXUS system) at 50 °C.

Cyclic voltammetry and electroplating experiments were conducted with an EG&G Princeton Applied Research Model 263A potentiostat/galvanostat controlled with EG&G PARC Model 270 software. A Pt disk electrode (Bioanalytica Systems, MF-2013, 0.02 cm^2) used as the working electrode, was polished to a mirror finish with a slurry of 0.3 μm alumina and then rinsed with distilled water and dry ethanol before use. A coil of ϕ1.0 mm Al wire (Alfa Aesar) was used as the counter electrode, which was immersed directly in the plating bath and encircled the working electrode. The reference electrode (Al/Al(III)) was constructed by placing a ϕ1.0 mm Al wire into a ϕ12 mm Pyrex tube terminated with a porosity glass frit (Ace Glass) and filling this tube with neat $AlCl_3$–EMI-Cl. The Al electrodes were cleaned with a mixture of concentrated H_2SO_4, HNO_3 and H_3PO_4, rinsed with distilled water and dried under vacuum before use. Copper wire (ϕ1.25 mm) served as the substrates for alloy electroplating, was electropolished at anodic current of 100 mA cm^{-2} in 0.236 M $CuSO_4$ aqueous solution for 1 min. Alloy samples of 5 μm thickness estimated by assuming that all of the charge produced an ordered layer of pure Al (14.5 C cm^{-2}), were deposited from ionic liquid solutions of Mo(II) and/or Ti(II) onto the Cu wire electrodes.

The surface morphology and crystal structure of electrodeposited alloy were observed with a scanning electron microscope (SEM, Keyence VE-8800) equipped with an energy dispersive X-ray fluorescence (EDX, EDAX VE-9800) spectrometer and examined by a X-ray diffractometer (XRD, RIGAKU X18 SAXS-IP) with CuKα radiation in a θ-2θ scan mode with scan rate of 2° min^{-1}. Pitting corrosion measurements were conducted on the resulting Al-Mo-Ti alloys by linear sweep voltammetry at room temperature in a 0.1 M NaCl aqueous solution. Some samples

were examined in a physiological saline solution composed of 137 mM NaCl + 2.7 mM KCl + 10 mM phosphate buffer at pH 7.4 and in Ringer's solution, which is composed of 38.5 mM NaCl + 1.41 mM KCl + 1.09 mM $CaCl_2 \cdot 2H_2O$ at pH 6.9. These measurements were carried out with an Ivium Technologies electrochemical interface CompactStat. Prior to these measurements, the solutions were thoroughly deaerated with nitrogen. Platinum foil and Ag/AgCl in saturated KCl solution were employed as the counter and reference electrodes, respectively. The potential values for this measurement are reported with respect to a NaCl-saturated calomel electrode (SSCE).

1-3. Results and Discussion

1-3-1. Reductive desorption of n-alkanethiol SAM in aqueous solution and ionic liquids

Figure 1-1 shows liner sweep voltammograms taken in 0.5 M KOH solution for Au(111) electrodes coated with *n*-alkanethiol SAM having different alkyl chain length. Each voltammogram shows a cathodic wave indicating reductive desorption of the alkanethiols, and its peak potential is negatively shifted and its width becomes narrower with an increasing in chain length. When the alkyl chain length of alkanethiol SAM increases, van der Waals interaction between alkyl chains becomes large, resulting in an increase in stability of the SAM. By considering such an interaction using an appropriate coordination model of adsorbed in alkanethiol molecules, Aoki and Kakiuchi have developed a method to numerically simulate the voltammogram of the reductive desorption of the alkanethiol SAM.[53, 89]

The same experiments were carried out in four kinds of ionic liquids. In order to compare the desorption potentials in different solutions, the redox potential of

ferrocene/ferricinium (Fc/Fc^+) couple was measured by cyclic voltammetry in each ionic liquid and all electrode potential were given respect to this redox potential. Figure 1-2 shows liner sweep voltammograms of the SAM-coated Au(111) electrodes taken in (a) EMI-BF_4, (b) BMI-BF_4, (c) EMI-TFSA and (d) BMI-TFSA. All voltammograms show definite cathodic waves, indicating clearly that electrochemical desorption of the alkanethiol SAM took place even in ionic liquids. In analogy with the case of the reductive desorption in aqueous solution, negative potential shifts were observed with an increase in the alkyl chain length. However, changes in shape of the cathodic wave were different from those in aqueous solution; the width tended to broaden as the alkyl chain became longer. The area of each cathodic wave was estimated by comparing the voltammogram for the SAM-coated Au(111) and that for a bare Au(111) taken in the same ionic liquid. The obtained values ranging from 0.69×10^{-9} to 0.79×10^{-9} mol cm^{-2} were close to the coverage (0.77×10^{-9} mol cm^{-2}) expected for a $(\sqrt{3} \times \sqrt{3})R30°$ overlayer structure of alkanethiols absorbed on the Au(111) surface.[44, 53-57, 90, 91] In voltammograms of *n*-decanethiol SAM-coated Au(111) taken in EMI-BF_4 and BMI-BF_4, shoulder peaks appeared with the main peaks . It has been reported by Poter et al. that such the peak splitting was observed even in aqueous solution especially for long alkanethiol SAM.[91] It was speculated that appearance of the peak splitting indicated presence of different structure in the SAM which have difference in accessibility of protons and/or electrolyte cationic species to the gold/sulfur interface. Similar argument might be made for voltammograms taken in ionic liquid but further investigation must be required for elucidation of the behavior.

Plots of peak potentials and peak widths of the cathodic waves as a function of chain length of the alkanethiol SAM are shown in Figure 1-3. The peak width at half

height was estimated using the voltammogram obtained for the naked Au(111) electrode as a base line. As mentioned above, however, cathodic waves obtained for decanethiol SAM in EMI-BF_4 and BMI-BF_4 exhibited shoulder peaks, making it difficult to determine precisely the main peak widths. It was attempted to remove the shoulder peaks with geometric means, but the values obtained by such the intentional treatment should include some errors. Then, the widths were estimated from five time experiments and they are given in Figure 1-3 with error bars. As mentioned above, negative shifts of the peak potential were observed for all cases, but the ratio of potential shift per increase in number of methylene unit was slightly different among the electrolytes used. The largest ratio was seen for aqueous KOH solution and it decreased in the order of BMI-BF_4, EMI-BF_4, EMI-TFSA and BMI-TFSA, as shown in Figure 1-3(a).

The relationship between peak width and alkyl chain length as shown in Figure 1-3(b) indicates clearly difference in the peak width changes among voltammograms taken in aqueous and ionic liquids. The width change tendencies could be classified into three types; decrease (in aqueous KOH solution; type I), no change (in EMI-BF_4 and BMI-BF_4; type II) and increase (in EMI-TFSA and BMI-TFSA; type III) with an increase in chain length. The type I is widely observed for electrochemical desorption of the alkanethiol SAM in aqueous solutions. In general, it was explained that stabilization of the SAM by the van der Waals interactions between alkyl chains concerns both negative peak potential shifts and the peak narrowing. However, it would be better to consider separately the effect of chain length on the peak potential shifts and that on the wave width for voltammograms obtained in ionic liquids. The results shown in Figure 1-3(b) suggest strongly that the anion species of the ionic liquids has a significant effect on the width of the cathodic wave.

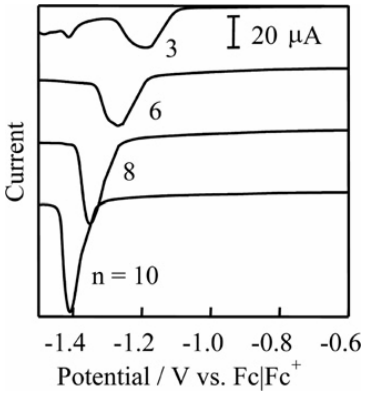

Figure 1-1. Linear sweep voltammograms for reductive desorption of self-assembled monolayer of *n*-alkanethiols having different chain lengths. All voltammograms were obtained in 0.5 M KOH aqueous solution with a scan rate of 0.1 V s^{-1}.

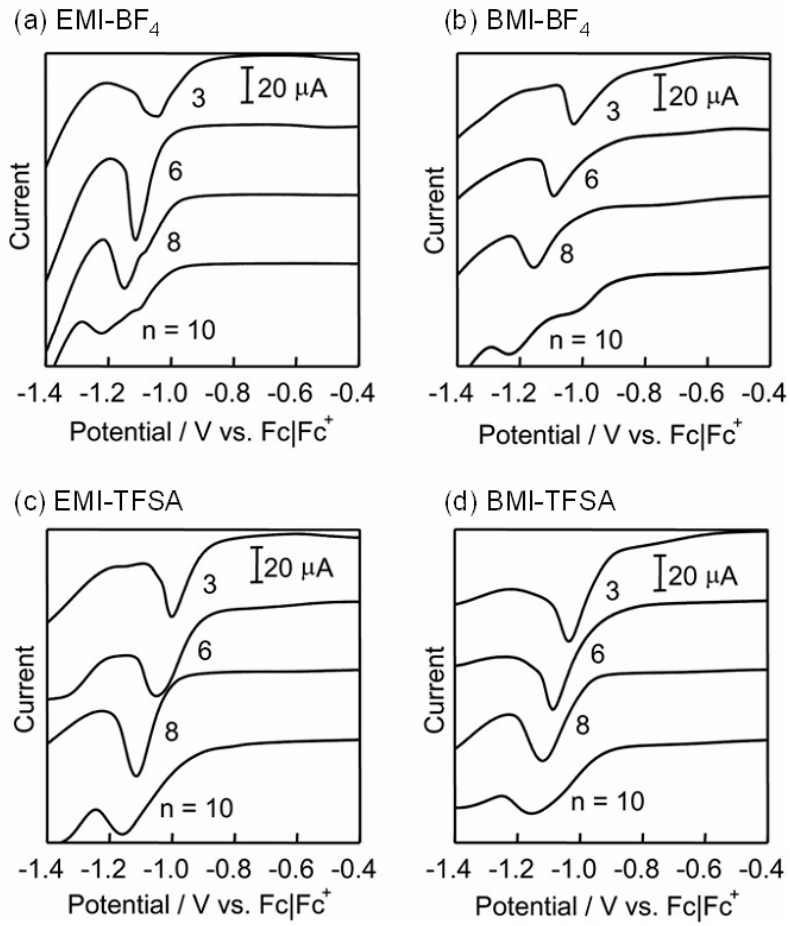

Figure 1-2. Linear sweep voltammograms for reductive desorption of SAM of *n*-alkanethiols (*n*-C_3H_7SH, *n*-$C_6H_{11}SH$, *n*-$C_8H_{17}SH$, and *n*-$C_{10}H_{21}SH$) obtained in ionic liquids (a) EMI-BF_4, (b) BMI-BF_4, (c) EMI-TFSA and (d) BMI-TFSA. The scan rate was 0.1 V s^{-1} for all voltammograms.

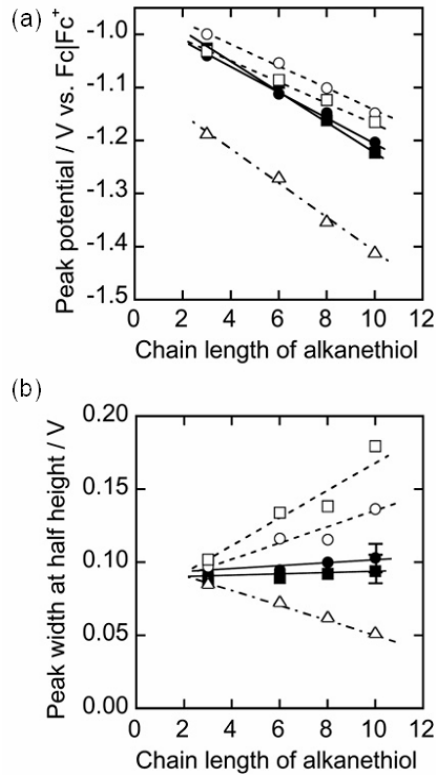

Figure 1-3. (a) Changes in peak potentials and (b) peak width at half height with increase in chain length. The reductive desorption of *n*-alkanethiol SAM was conducted in 0.5 M KOH aqueous solution (Δ) and ionic liquids (EMI-BF_4(●), BMI-BF_4(■), EMI-TFSA (○) and BMI-TFSA (□)).

1-3-2. Numerical simulation of reductive desorption of n-alkanethiol SAM

In order to understand the above-mentioned effects of chain length on reductive desorption of the alkanethiol SAM in ionic liquids, the numerical simulation was attempted using the method developed by Aoki and Kakiuchi, which expressed the reductive desorption behavior of the alkanethiol SAM based on a model of hexagonally packed thiol molecules as shown in Scheme 1-1. Before desorption, one thiol molecule is surrounded by six thiol molecules. When the thiol molecule is stabilized by a neighboring thiol molecule with the stabilization energy of u_R, the thiol molecule in a perfect SAM in stabilized by 6 u_R. It is assumed here that the center thiol molecule

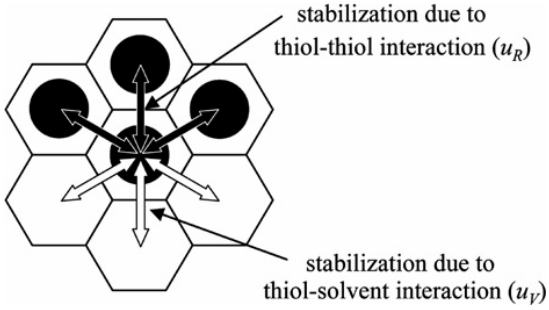

Scheme 1-1. The honeycomb model used for numerical calculation of linear sweep voltammograms. In this case, the center thiol molecule is stabilized by three neighboring thiol molecules ($-3u_R$) and three vacancy sites occupied by solvent molecules ($-3u_V$), respectively.

remains, while the surrounding thiol molecules are desorbed, allowing solvent molecules to occupy the generated vacancy sites. If the stabilization energy of the center thiol molecule by the solvent is denoted by u_V, desorption of one thiol molecule changes the total stabilization energy for the center thiol molecule to $5u_R + u_V$. The energy is then continuously changed to $4u_R + 2u_V$, $3u_R + 3u_V$, $2u_R + 4u_V$, $u_R + 5u_V$, and $6u_V$ with progress of the desorption. Based on such a model, the electrode potential (E) and current (I) can be formulated as functions of the coverage of thiol SAM (x)

$$E = E^0 - \frac{RT}{\alpha F}\ln\left\langle \frac{\alpha F v}{k\Gamma \exp\left(\frac{6u_V}{k_B T}\right) RT}\left\{\ln\frac{wx+1}{(w+1)x} + \sum_{n=1}^{5}\left[\frac{1}{n(w+1)^n} - \frac{1}{n(wx+1)^n}\right]\right\}\right\rangle \quad (2)$$

$$I = -F\Gamma\frac{\alpha F v}{RT}\left\{\ln\frac{wx+1}{(w+1)x} + \sum_{n=1}^{5}\left[\frac{1}{n(w+1)^n} - \frac{1}{n(wx+1)^n}\right]\right\}x(wx+1)^6 \quad (3)$$

$$\left(w = \exp\left(\frac{u_R - u_V}{k_B T}\right) - 1\right)$$

where E^o is the standard electrode potential of the desorption reaction, R is the gas constant, T is the absolute temperature, F is Faraday's constant, α is the transfer

coefficient (0.84 in this case),[89] k is the rate constant of the desorption reaction, Γ is the surface density of the closely packed thiol SAM (0.77×10^{-9} mol cm^{-2}), k_B is the Bolzmann constant and v is rate of potential scan. Values of E and I are obtained by substituting values from 1 to 0 into x in eq. (2) and (3). Then, plots of I values as a function of E give a simulation curve of the linear sweep voltammogram.

In the case of desorption in aqueous solution, it is assumable that solvent is the same even if supporting electrolyte and solution pH are different. Based on this assumption, in the first paper regarding this model,[89] $u = u_R - u_V$ is treated as the parameter representing the interaction energy between alkanethiol molecules relative to the energy between alkanethiol molecules and vacant, which takes always negative value. However, when ionic liquid containing no solvent is used as an electrolyte, it is required to consider that the u_V is changed by changing kind of ionic liquid used as an electrolyte.

Simulated voltammogram curves exhibit how u_R and u_V influence the peak potential and the shape of the cathodic wave of the voltammogram. Some typical examples are shown in Figure 1-4. The negative shift of the u_R value with an increase in chain length means more stabilization of the SAM due to van der Waals interaction between alkyl chains. Increase in chain length also increase numbers of solvent molecules that can touch to alkyl chains, resulting in proportional changes in u_V value to the chain length. As shown in Figure 1-4, negative shift of both u_R and u_V with alkyl chain length causes negative shift of the peak potential, while relationship between u_R and u_V values determines tendency of the width changes. As mentioned previously, the electrochemical desorption of alkanethiol SAM in the ionic liquids was classified to three types. The simulated voltammograms shown in Figure 1-4 seem to express well

the three types; Figure 1-4(a), (b), and (c) depict the voltammograms belonging to the types I, II and III, respectively.

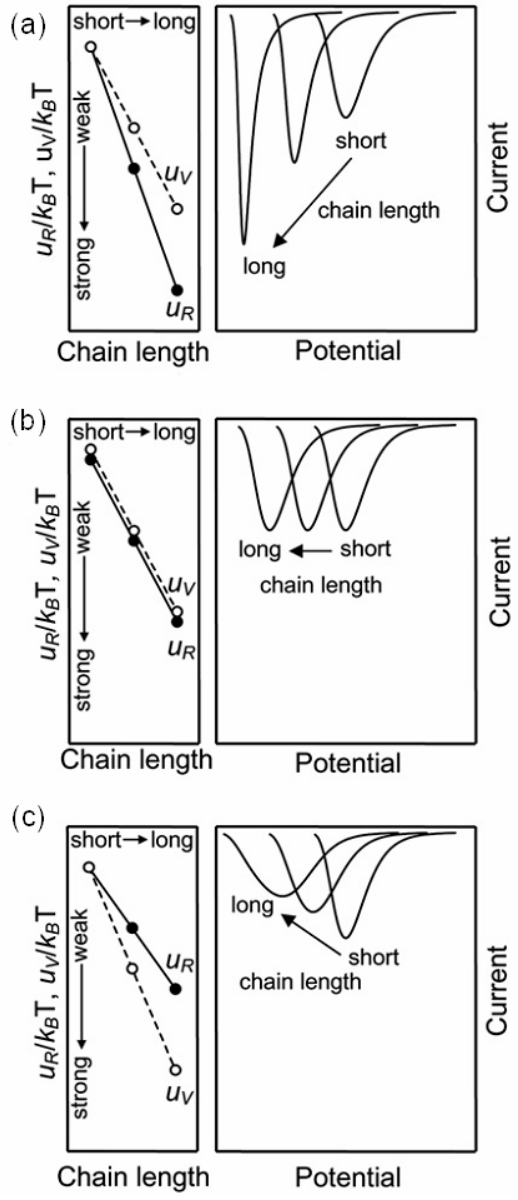

Figure 1-4. Changes in potential and width of simulated desorption peak with increase in stabilizing energies due to thiol-thiol (u_R) and thiol-solvent (u_V) interactions in the cases of (a) $\Delta u_R > \Delta u_V$, (b) $\Delta u_R = \Delta u_V$ and (c) $\Delta u_R < \Delta u_V$.

1-3-3. Plausible reaction model for SAM desorption in ionic liquids

The comparison of experimentally obtained voltammograms shown in Figure 1-2 and numerically simulated voltammograms shown in Figure 1-4 gives several hints for considering reductive desorption behavior of the alkanethiol SAM. The alkanethiol SAM is definitely desorbed by electrochemical reduction even in ionic liquid but it is required to consider that the reaction takes place under the condition without any solvent. Negative charges of the desorbed alkanethiolate molecules are, of course, compensated by cationic species of ionic liquid. However, both anionic and cationic species should concern dissolution of the alkanethiolate molecules. In addition, the both species also should interact with the alkanethiol SAM on the Au electrode, as shown in Scheme 1-2. In other words, although the parameter u_V concerns interaction between the alkyl chains of the SAM and solvent for the desorption in aqueous solution, it must concern interaction between alkyl chains of the SAM and anionic and cationic species in the case of the desorption in ionic liquids.

The most notable influence of ionic liquid on the SAM desorption is that anionic species determines the desorption behavior; the desorption in ionic liquids containing BF_4^- belongs to the type II and the reaction in ionic liquids containing $TFSA^-$ belongs to the type III. As well known, EMI-BF_4 and BMI-BF_4 commingle with water but EMI-TFSA and BMI-TFSA are completely separated from water, indicating that anionic species, i.e. BF_4^- and $TFSA^-$ determine hydrophobicity of the four ionic liquids used in this study. This fact allows me to speculate that $TFSA^-$ possessing more hydrophobicity than BF_4^- interacts more strongly with alkyl chain of the SAM and dissolved alkanethiolate. Such the situation might enlarge slope of the changes in u_V value with an increase in chain length of the SAM. It was a little difficult to estimate

precisely the slope of u_V changes and that of u_R changes from the voltammograms obtained in this study. However, it is likely that higher interaction between $TFSA^-$ and the alkyl chain of the SAM is the main reason why the cathodic peak broadened with an increase in alkyl chain length. Although the ionic liquids of BF_4^--salts are mixed with water, hydrophobicities of this organic species must be higher than that of water. Therefore, the slope of u_V changes for these ionic liquids might be larger than that for water, resulting in almost no changes in cathodic wave width.

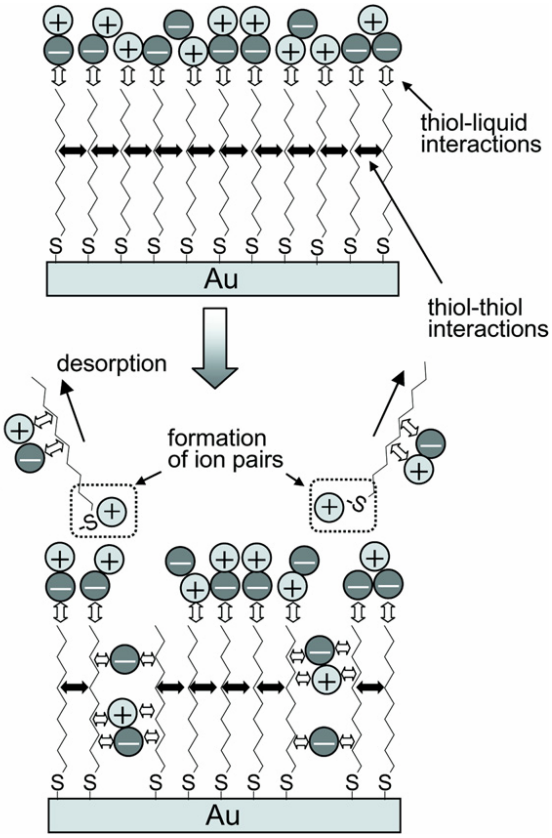

Scheme 1-2. Schematic illustration of proposed mechanism of reductive desorption of SAM in ionic liquid.

1-3-4. Voltammetric behavior of $AlCl_3$–EMI-Cl ionic liquid

Figure 1-5(a) shows cyclic voltammograms recorded at a Pt rotating disk electrode (Pt-RDE, 2000 rpm) in 66.7-33.3 mol% $AlCl_3$–EMI-Cl before and after the addition of $(Mo_6Cl_8)Cl_4$ and $TiCl_2$. Al deposition occurs by the electrochemical reduction of the coordinately unsaturated $Al_2Cl_7^-$ ion in the ionic liquid according to the equation.[92]

$$4Al_2Cl_7^- + 3e^- \leftrightarrows 7AlCl_4^- + Al$$

When Mo(II) or Ti(II) is present in the ionic liquid, this reaction becomes

$$xM(AlCl_4)_p^{(p-2)-} + 4(1-x)Al_2Cl_7^- + (3-x)e^- \leftrightarrows Al_{1-x}M_x + [7(1-x) + px]AlCl_4^-$$

where $M(AlCl_4)_p^{(p-2)-}$ presents Mo(II) or Ti(II) solvated in the chloroaluminate ionic liquid by $AlCl_4^-$ and $Al_{1-x}M_x$ denotes the resulting aluminum-transition metal alloy. In

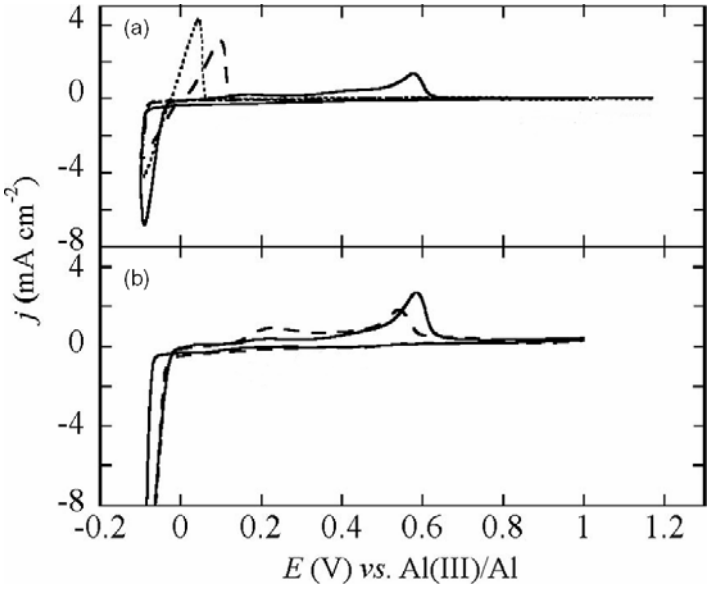

Figure 1-5. Cyclic voltammograms recorded at a Pt-RDE (2000 rpm) in 66.7-33.3 mol% $AlCl_3$–EMI-Cl: (a) (···) pure ionic liquid, (—) 15 mM Mo(II), (---) 15 mM Ti(II); (b) (—) 30 mM Mo(II) + 15 mM Ti(II), (---) 15 mM Mo(II) + 30 mM Ti(II). The scan rates were 0.05 V s^{-1}, and the temperatures were 323 K.

the pure ionic liquid, a stripping wave for electrodeposited Al begins at around 0 V, but this wave is replaced by waves corresponding to the stripping of the electrodeposited Al-Mo and Al-Ti alloys in the solutions containing Mo(II) or Ti(II), respectively.[78, 80] Cyclic voltammograms recorded in the ionic liquid containing both Mo(II) and Ti(II) are shown in Figure 1-5(b). Regardless of the Mo(II)/Ti(II) concentration ratio, $C_{Mo(II)}/C_{Ti(II)}$, these voltammogram are more or less similar in appearance to that recorded in the Mo(II) solution. This implies that the formation of Al-Mo dominates the ternary Al alloy deposition process.

1-3-5.Preparation and characterization of Al-Mo-Ti alloys

Alloy samples were deposited on cupper rotating wire electrode substrates under constant current conditions at a rotation rate of 2000 rpm. The various alloy samples that were produced and the deposition conditions used to produce them are given in Table 1-1. Figure 1-6 shows the variation in the Mo and/or Ti content of the resulting Al-Mo, Al-Ti and Al-Mo-Ti electrodeposits as a function of the applied current density. In the case of the binary alloys that were prepared in solutions containing either Mo(II) or Ti(II), the Mo content of the Al-Mo is always significantly greater than the Ti content of the corresponding Al-Ti alloys even when the two binary alloys were prepared under identical conditions of applied current density, electrode rotation rate, concentration of the precursor ions and temperature. As shown in Table 1-1 and Figure 1-6, this same result carries over to the ternary alloys, including those prepared with $C_{Mo(II)} = C_{Ti(II)}$, because the Ti content of these alloys is always significantly smaller than the Mo content.

This result can be reconciled by considering the diffusion coefficients of Mo(II)

Table 1-1. Summary of Al-Mo-Ti Alloys electrodeposited from 66.7-33.3 mol% $AlCl_3$–EMI-Cl.

Deposition conditions[a]			Alloy properties		Pitting potential[b,c] (V vs SSCE)		
Current density (mA cm^{-2})	$C_{Mo(II)}$ (mmol L^{-1})	$C_{Ti(II)}$ (mmol L^{-1})	Mo content (atom %)	Ti content (atom %)	NaCl solution	Buffer solution[d]	Ringer's solution[e]
−10	30	—	8.7	—	—	−0.051	—
−20	30	—	8.0	—	—	—	—
−40	30	—	6.2	—	−0.061	—	—
−80	30	—	3.2	—	—	—	−0.011
−5	—	30	—	3.7	—	—	−0.261
−10	—	30	—	3.1	—	—	—
−20	—	30	—	2.2	—	—	—
−40	—	30	—	1.5	−0.031	—	—
−80	—	30	—	1.0	—	−0.371	—
−10[f]	35.5	—	9.9	—	0.042	—	—
−10[g]	—	170	—	15.7	−0.262	—	—
−5	30	15	9.7	0.7	—	—	—
−10	30	15	8.4	0.6	0.059	—	—
−20	30	15	6.0	0.7	—	0.039	—
−40	30	15	6.0	0.6	—	—	0.069
−80	30	15	2.9	0.6	—	—	—
−5	30	30	6.9	0.7	0.049	—	—
−10	30	30	5.7	0.7	—	−0.031	—
−20	30	30	5.3	0.7	—	—	−0.101
−40	30	30	3.2	0.8	—	—	—
−80	30	30	1.6	0.4	−0.191	—	—
−5	15	30	6.7	0.8	—	—	—
−10	15	30	3.9	0.8	—	—	—
−20	15	30	2.0	0.7	−0.131	—	—
−40	15	30	2.0	0.7	—	−0.201	—
−80	15	30	1.1	0.6	—	—	−0.321

[a] 2000 rpm, 323 K.
[b] 0.5 mV s^{-1}, 298 K.
[c] The pitting potential of pure Al in the NaCl solution is −0.683 V vs SSCE.
[d] 137 mmol L^{-1} NaCl + 2.7 mmol L^{-1} KCl + 10 mmol L^{-1} phosphate buffer solution (pH 7.4 at 298 K).
[e] 38.5 mmol L^{-1} NaCl + 1.41 mmol L^{-1} KCl + 1.09 mmol L^{-1} $CaCl_2 \cdot 2H_2O$ (pH 6.9 at 298 K).
[f] 2000 rpm, 328 K.
[g] 500 rpm, 353 K.

and Ti(II), $D_{Mo(II)}$ and $D_{Ti(II)}$, respectively, in the ionic liquid. Although there are no direct measurements of these diffusion coefficients under the exact experimental conditions employed herein, a rough estimate of $D_{Mo(II)}/D_{Ti(II)}$ can be obtained from the ratio of the Stokes-Einstein products for Mo(II) and Ti(II). The Stokes-Einstein product, $D\eta/T$, where D (cm^2 s^{-1}) represents the diffusion coefficient of the electroactive species, η (g cm^{-1} s^{-1}) is the absolute viscosity of the ionic liquid, T (K) is the absolute temperature, is inversely proportional to the radius of the diffusing entity in the solvent. All conditions being equal, an ion or molecule with a larger $D\eta/T$ is expected to diffuse more rapidly than the species with a smaller $D\eta/T$. For a Ti(II) concentration of 12.6 mM, $D_{Ti(II)}\eta/T = 3.1 \times 10^{-11}$ g cm s^{-2} K^{-1} in the 66.7-33.3 mol% $AlCl_3$–EMI-Cl ionic

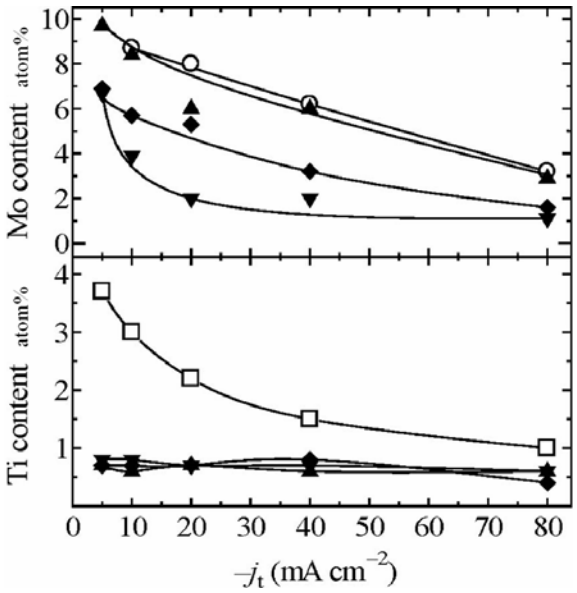

Figure 1-6. The relationship between the plating current density and the percent atomic fraction of Mo (upper panel) and Ti (lower panel) in the deposits. The solution compositions were: (○) 30 mM Mo(II); (□) 30 mM Ti(II); (▲) 30 mM Mo(II) + 15 mM Ti(II); (♦) 30 mM Mo(II) + 30 mM Ti(II); (▼) 15 mM Mo(II) + 30 mM Ti(II). The substrate rotation rates were 2000 rpm and the temperatures were 323 K.

liquid.[80] It is necessary to report the Ti(II) concentration at which the measurements of $D_{Ti(II)}\eta/T$ were carried out because this species is known to form polymeric or aggregated species, $[Ti(II)]_n$, as the Ti(II) concentration is increased.[93] This indicates that the radius of the diffusing Ti(II) increases as its concentration is increased.

In order to obtain more insight into the Al-Mo-Ti deposition process, the composition data in Figure 1-6 were converted to partial current densities by using the following expressions,

$$j_{Mo} = j_t n_{Mo} x_{Mo} / (n_{Mo} x_{Mo} + n_{Ti} x_{Ti} + n_{Al} x_{Al})$$

$$j_{Ti} = j_t n_{Ti} x_{Ti} / (n_{Mo} x_{Mo} + n_{Ti} x_{Ti} + n_{Al} x_{Al})$$

$$j_{Al} = j_t - j_{Mo} - j_{Ti}$$

where j_t is the total applied current density; j_{Mo}, j_{Ti} and j_{Al} represent the partial current

densities for Mo, Ti and Al, respectively; n_{Mo}, n_{Ti} and n_{Al} represent the number of electrons involved in the alloy deposition: 2, 2 and 3, respectively; and x_{Mo}, x_{Ti} and x_{Al} are the atomic fractions of Mo, Ti and Al in the alloys, respectively. Plots of $-j_{Mo}$, $-j_{Ti}$ and $-j_{Al}$ vs. $-j_t$ are shown in Figure 1-7, indicating that $-j_{Al}$ varies almost linearly with $-j_t$, whereas the plots of $-j_{Mo}$ vs. $-j_t$ and $-j_{Ti}$ vs. $-j_t$ display a more complex behavior. For example, $-j_{Mo}$ increases at low values of $-j_t$, but reaches a limiting value as $-j_t$ is increased. This behavior explains why the Mo content of the Al-Mo and Al-Mo-Ti alloys decreases as $-j_t$ is increased because once $-j_{Mo}$ reaches a limiting value, it becomes a smaller fraction of $-j_t$, whereas $-j_{Al}$ becomes an increasingly larger fraction of $-j_t$ as the latter is increased. This result was noted during studies on the

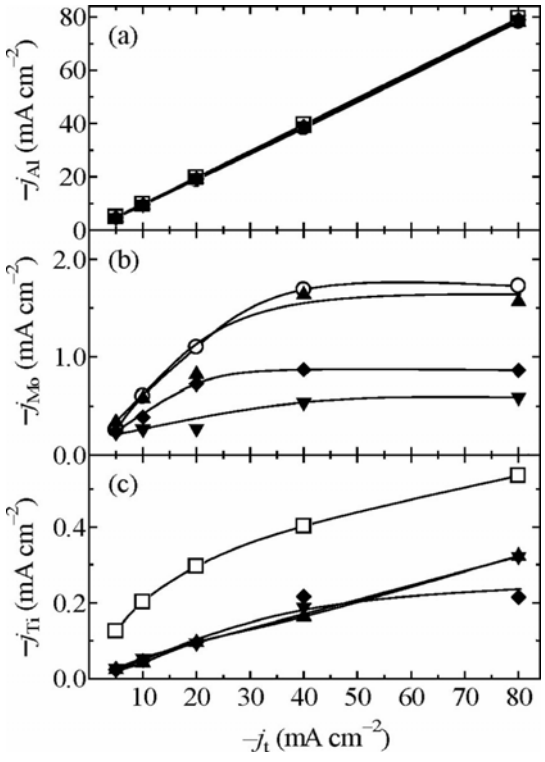

Figure 1-7. Plots of the partial current densities for the deposition of (a) Al, (b) Mo and (c) Ti vs. the total current density as calculated from the composition data in Figure 1-6. The solution compositions were: (○) 30 mM Mo(II); (□) 30 mM Ti(II); (▲) 30 mM Mo(II) + 15 mM Ti(II); (♦) 30 mM Mo(II) + 30 mM Ti(II); (▼) 15 mM Mo(II) + 30 mM Ti(II).

electrodeposition of Al-Mo[78] and Al-Mo-Mn[79] from the same ionic liquid, and it is based on the fact that the concentration of Mo(II) in the solvent is much smaller than the concentration of the reducible Al(III) species, $Al_2Cl_7^-$. Figure 1-7 also shows that $-j_{Ti}$ generally increases with $-j_t$, but always remains considerably smaller than either $-j_{Mo}$ or $-j_{Al}$ as expected based the substantial difference between $D_{Mo(II)}$ and $D_{Ti(II)}$.

SEM images of some Al-Mo-Ti alloy samples are shown in Figure 1-8. Figure 1-8(a) and (b) depict the surface morphology of Al-Mo-Ti alloys prepared at different

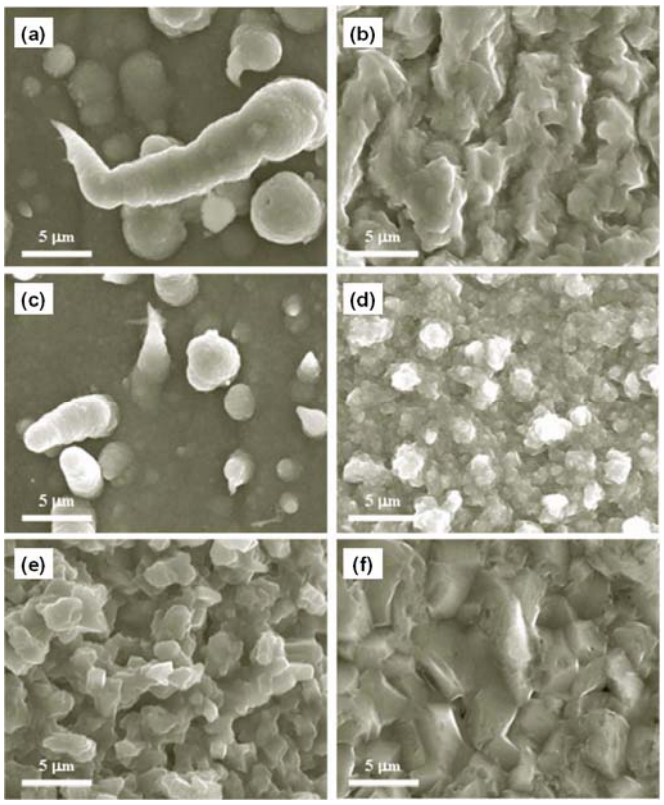

Figure 1-8. SEM images of electrodeposited Al-Mo-Ti alloy samples. The alloy compositions, current densities, and solution compositions were: (a) $Al_{89.6}Mo_{9.7}Ti_{0.7}$, −5 mA cm^{-2}, 30 mM Mo(II) + 15 mM Ti(II); (b) $Al_{93.3}Mo_{6.0}Ti_{0.7}$, −20 mA cm^{-2}, 30 mM Mo(II) + 15 mM Ti(II); (c) $Al_{92.4}Mo_{6.9}Ti_{0.7}$, −5 mA cm^{-2}, 30 mM Mo(II) + 30 mM Ti(II); (d) $Al_{94.0}Mo_{5.3}Ti_{0.7}$, −20 mA cm^{-2}, 30 mM Mo(II) + 30 mM Ti(II); (e) $Al_{92.5}Mo_{6.7}Ti_{0.8}$, −5 mA cm^{-2}, 15 mM Mo(II) + 30 mM Ti(II); and (f) $Al_{97.3}Mo_{2.0}Ti_{0.7}$, −20 mA cm^{-2}, 15 mM Mo(II) + 30 mM Ti(II).

current densities under the condition of $C_{Mo(II)}/C_{Ti(II)} = 2$. The surface of alloy produced at –5 mA cm^{-2} ($Al_{89.6}Mo_{9.7}Ti_{0.7}$) shown in Figure 1-8(a) is covered with elongated carrot-shaped, dendritic nodules from 2 to 4 μm diameters. Deposits prepared at –20 mA cm^{-2} ($Al_{93.3}Mo_{6.0}Ti_{0.7}$) consist of asymmetric, fused nodules without crystallographic faces (Figure 1-8(b)). Deposits prepared at –5 mA cm^{-2} with $C_{Mo(II)}/C_{Ti(II)} = 1$ ($Al_{92.4}Mo_{6.9}Ti_{0.7}$, Figure 1-8(c)) are similar in structure to those appearing in Figure 1-8(a), but the nodules are somewhat smaller. A deposit prepared at –20 mA cm^{-2} in the same plating bath ($Al_{94.0}Mo_{5.3}Ti_{0.7}$, Figure 1-8(d)) consists of small fused nodules with crystalline characteristics. When the plating bath was adjusted $C_{Mo(II)}/C_{Ti(II)} = 0.5$, alloy deposit prepared at –5 mA cm^{-2} ($Al_{92.5}Mo_{6.7}Ti_{0.8}$) exhibits a macroporous structure (Figure 1-8(e)). Deposited prepared at –20 mA cm^{-2} in the same solution ($Al_{97.3}Mo_{2.0}Ti_{0.7}$) display a fused leaflike structure which is very similar to pure Al, probably because of their relatively low transition metal content (Figure 1-8(f)).[94]

The crystal structure of several electrodeposited alloy samples were examined with XRD techniques and the diffraction patterns are shown in Figure 1-9. In all cases, the diffraction patterns could be indexed to face centered cubic (fcc) Al and the underlying Cu substrate. Considering that the solid solubility of Mo and Ti in pure Al is quite small; around 0.001 atom% at 833 K for Mo and 0.14 atom% at 783 K for Ti,[95] the Al-Mo-Ti alloys prepared herein must be supersaturated solid solutions with fcc Al structure. Before examining these deposits with XRD techniques, it was expected that this ternary alloy system would form amorphous metallic glasses similar to those found for Al-Mo[78] and Al-Mo-Mn.[79] The formation of amorphous deposits was found to occur when the Mo content of these alloys exceeds 8 atm%, and it is usually signaled by the disappearance of the fcc Al reflections and the development of a broad reflection

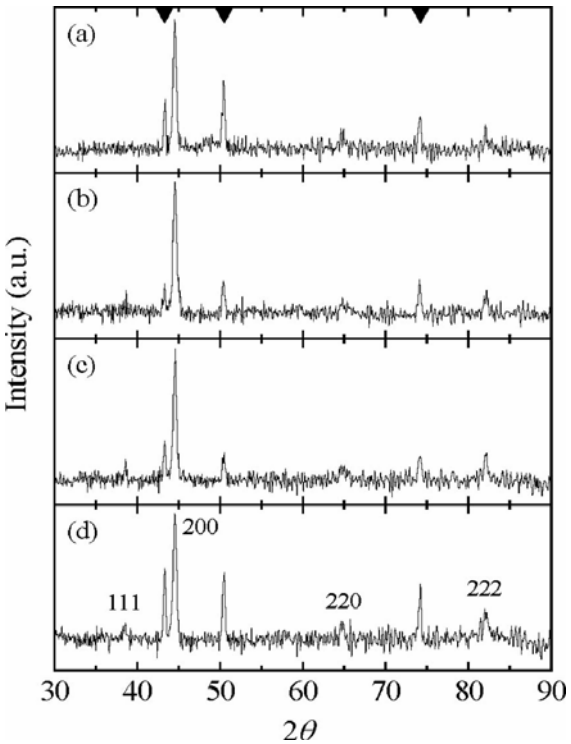

Figure 1-9. X-ray (Cu Kα) diffraction data of Al-Mo-Ti alloys: (a) $Al_{89.6}Mo_{9.7}Ti_{0.7}$, (b) $Al_{93.4}Mo_{6.0}Ti_{0.6}$, (c) $Al_{96.0}Mo_{3.2}Ti_{0.8}$, and (d) $Al_{97.3}Mo_{2.0}Ti_{0.7}$. Reflections from the Cu substrate are denoted by (▼).

centered at about 2θ = 41°. However, even when the total Mo content of the Al-Mo-Ti deposit approached 10 atom% (Figure 1-9(a)), there was no obvious evidence of a metallic glass phase. Given that no amorphous Al-Ti alloy has been reported to date,[80] it is likely that Ti atoms in the Al-Mo-Ti alloys act as a barrier to metallic glass formation.

1-3-6. Corrosion resistance test of electrodeposits

It is well known that nonequilibrium Al-transition metal alloys are more resistant to chloride-induced pitting corrosion than pure Al.[82, 83] Furthermore, previous research has shown that such alloys prepared by isothermal electrodeposition in chloroaluminate ionic liquids have almost the same pitting potentials as similar alloys

prepared by other nonequilibrium alloying method, such as rapid solidification, ion implantation and sputter deposition.[78-81]

The corrosion resistance of several electrodeposited Al-Mo-Ti alloys was examined by linear sweep voltammetry in a deaerated 0.1 M NaCl aqueous solution, shown in Figure 1-10. The Al-Mo-Ti alloys are spontaneously passive at the rest potential in the measuring solution and sustain a stable passive region, followed by a sudden rise in current at the pitting potential. The resulting variation of the pitting potential is collected in Table 1-1 and displayed graphically in Figure 1-11 along with selected data for the binary alloys, Al-Mo[78] and Al-Ti.[80] The Al-Mo-Ti alloys display higher corrosion resistance than the Al-Ti binary alloys and compete with Al-Mo alloys, regardless of the overall transition metal content (Mo + Ti). For example, the pitting

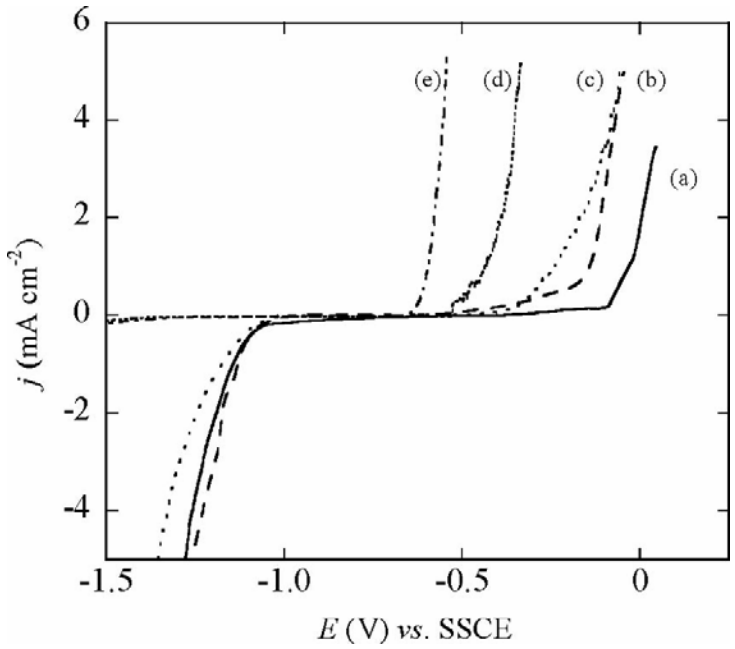

Figure 1-10. Anodic polarization curves recorded in deaerated 0.1 M NaCl aqueous solution for (a) $Al_{92.4}Mo_{6.9}Ti_{0.7}$, (b) $Al_{93.8}Mo_{6.2}$, (c) $Al_{97.3}Mo_{2.0}Ti_{0.7}$, (d) $Al_{97.8}Ti_{2.2}$ and (e) pure Al. The scan rates were 0.5 mV s^{-1}, and the temperatures were 298 K.

potential for the $Al_{98.0}Mo_{1.6}Ti_{0.4}$ alloy sample is 0.07 V more positive than that for $Al_{84.3}Ti_{15.7}$. Similarly, the pitting potential for $Al_{97.3}Mo_{2.0}Ti_{0.7}$ is comparable to that for the $Al_{94.9}Mo_{5.1}$. Thus, it follows that the addition of a second transition element, either Mo or Ti to Al-Ti or Al-Mo, respectively, results in a ternary alloy with superior corrosion resistance compared to the corresponding binary alloy. However, the pitting potential of the best Al-Mo-Mn alloy electrodeposited from 66.7-33.3 mol% $AlCl_3$–EMI-Cl ionic liquid, $Al_{89.5}Mo_{9.1}Mn_{1.4}$,[79] is 0.095 V greater than that of the best Al-Mo-Ti alloy, $Al_{91.0}Mo_{8.4}Ti_{0.6}$. The difference in pitting potentials may be attributed to the fact that the former forms a metallic glass phase, whereas the latter does not appear to do so.

Figure 1-12 shows SEM images of $Al_{91.0}Mo_{8.4}Ti_{0.6}$ before and after pitting potential measurements. As expected, the anodic polarization experiments resulted in considerable modification of the surface morphology of the alloy deposit; the dense, smooth surface with spherical and/or elongated cone-shaped nodules in Figure 1-12(a)

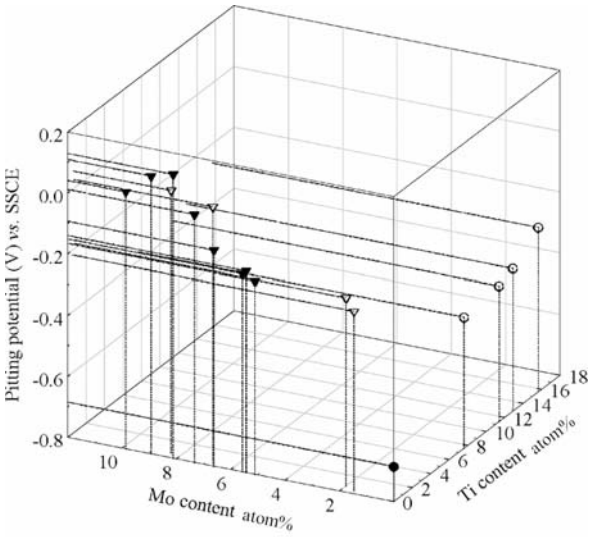

Figure 1-11. Pitting potentials of electrodeposited Al-Mo-Ti alloys: (●) pure Al, (○) Al-Ti, (▼) Al-Mo, and (▽) Al-Mo-Ti.

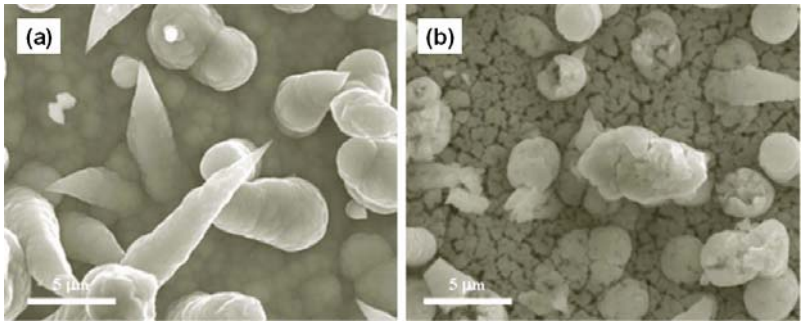

Figure 1-12. SEM images of $Al_{91.0}Mo_{8.4}Ti_{0.6}$ (a) before and (b) after the anodic polarization measurements in Figure 1-11

.

changes to a spongy appearance after the measurements as Figure 1-12(b). EDX analysis of the deposit shown in Figure 1-12(b) indicated a sharp increase in the surface concentration of Mo and Ti, indicating that Al was the primary element stripped from these alloy deposits during the anodic polarization experiments. Similar results were found during a previous investigation involving Al-Mo binary alloys.[78]

Polarization measurements were also carried out in simulated body fluids using the two solutions; physiological saline and Ringer's solutions, because some alloys based on Al and Ti are useful biomedical and dental implant materials. The results are also given in Table 1-1, but there is not much difference between these data and those recorded in the NaCl solution. By comparison, the pitting potentials of typical Al alloys that are used as biomaterials such as $Al_{54.6}Ti_{9.1}V_{36.3}$ and $Al_{42.9}Ti_{7.1}Nb_{50.0}$ are around 1.50 V vs SCE.[96] These materials contain a much greater proportion of the transition metal component than the Al-Ti-based alloys that can be prepared from the $AlCl_3$–EMI-Cl ionic liquid and are also much more resistant to chloride-pitting corrosion.

1-4. Conclusions

It has been clarified that ionic liquids without any solvent could be used as electrolyte solution for electrochemical reductive desorption of alkanethiol SAM and electrochemical deposition of aluminum-transition metal alloy.

In KOH aqueous solution, the peak potentials shifted in a negative direction and peak width narrowed with an increase in alkyl chain length of the SAM. This means that the stabilizing energy due to thiol-thiol interaction became dominant compared to that due to thiol-solvent (water) interaction. On the other hand, although negative shifts of the peak potential with an increase in chain length were also observed in voltammograms taken in all ionic liquids, the peak width was not notably changed in EMI-BF_4 and BMI-BF_4, and the peak widths broadening were observed in EMI-TFSA and BMI-TFSA. Considering the desorption reaction in the ionic liquids used in this study, it is likely that anionic species of the ionic liquids work as solvent and cationic species work as charge compensators of alkanethiolate generated by the electrochemical desorption.

The electrodeposition of Al-Mo-Ti ternary alloys containing up to 9.7 atom% Mo and 0.7 atom% Ti was achieved in the 66.7-33.3 mol% $AlCl_3$–EMI-Cl ionic liquid containing $(Mo_6Cl_8)Cl_4$ and $TiCl_2$. When Mo(II) and Ti(II) coexisted in the plating bath, it was not possible to prepare alloy deposits containing more than 1 atom% Ti. Thus, Mo(II) strongly suppresses the codeposition of Ti. Nevertheless, the chloride pitting corrosion resistance of Al-Mo-Ti containing small amounts of Ti was superior to binary Al-Mo alloys with a similar or even larger Mo content.

Chapter 2

Scanning Electron Microscope Observation of Insulating Materials Using Ionic Liquids as Antistatic Agents

2-1. Introduction

Since electron microscope observation requires placing specimen in a vacuum chamber, it is impossible to observe a wet sample as it is. Even if a low-vacuum scanning electron microscope is used, a wet sample like biomaterial must be frozen during observation. Furthermore, it is required for insulating samples to be subjected to pretreatments such as coating of metal and carbon by vapor deposition or sputtering under vacuum condition to avoid charging of the sample during observation. The finding that ionic liquids behave like an electronic conducting material for electron microscope observation[34-36] let to have got an idea of observing samples wetted by ionic liquids having electronic conductivity. In this chapter, I will introduce some ways to use ionic liquids for SEM observation. It will be shown that ionic liquids are useful for putting electronic conductivity to insulating materials without any special instrument. This technique is easily applied to biomaterials such as brown seaweed, whose morphology is changed by including much water. First, abrasive paper and absorbent cotton were observed as the sample having a rough surface and a complicated three-dimensional structure, respectively.

2-2. Experimental

Ionic liquids of 1-butyl-3-methylimidazolium tetrafluoroborate (BMI-BF_4), and 1-butyl-3-methylimidazolium bis(trifluoromethanesulfonyl)amide (BMI-TFSA) were treated by the same procedure described in chapter 1 prior to use. Water used for swelling of seaweed was purified using a Milli-Q water system (Millipore Corporation). Abrasive paper, absorbent cotton and dry seaweed were purchased on the market. Coating of insulating samples with gold was conducted by a sputter coater (Eiko, IB-3). A scanning electron microscope used in this work was Keyence VE-8800 SEM. The probe current and the electron dose for SEM observation are 4.0×10^{-10} A and 2.4×10^{-8} C ml^{-1} (ionic liquid), respectively, at most.

2-3. Results and Discussion

2-3-1. SEM observation of insulating materials

Utilization of ionic liquid for putting electronic conductivity to an insulating sample was examined using a # 150 abrasive paper. Of course, this insulating sample as is gave a bright SEM image with lots of noises, as shown in Figure 2-1(a). Then, coating it with metal or carbon is necessary to obtain its clear image as shown in Figure 2-1(b). Figure 2-1 (c) shows a SEM image of the same abrasive paper, surface of which was coated with ionic liquid of BMI-TFSA in place of gold. The coating was made by putting the sample in BMI-TFSA, and excess amount of the liquid was removed by a tissue paper. The sample was not charged at all, as expected. However, some amount of the ionic liquid remained, hiding the concave portions because SEM could only observe the surface of the sample. Then, the real roughness of the sample surface could not be

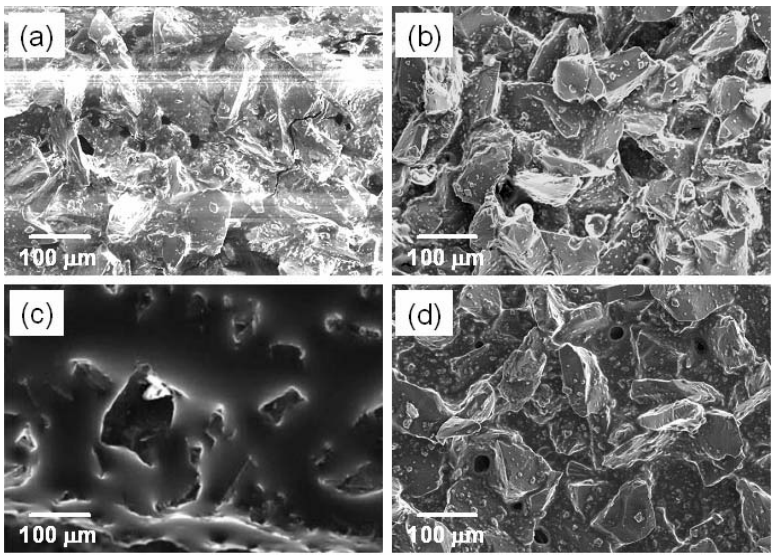

Figure 2-1. SEM images of surfaces of #150 abrasive paper (a) without any treatment, coated with (b) gold (c) neat BMI-TFSA and (d) BMI-TFSA/ethanol solution. The accelerate voltage for SEM observation was 20 kV.

clearly observed. This unfortunate situation was met even if different kind of ionic liquid having low-viscosity was used. Among several attempts for erasing the ionic liquid pools from the sample surface, dilution of ionic liquid worked most effectively. In this case, BMI-TFSA was diluted by ethanol so as to give concentration of 2.0 M and the abrasive paper was dipped in this solution, followed by evaporation of ethanol in air. The resulting SEM image as shown in Figure 2-1(d) and the image of gold-coated sample (Figure 2-1(b)) have no significant difference, indicating that very thin ionic liquid layer coated on the sample surface and it worked effectively as an antistatic agent for SEM observation with a high accelerating voltage.

As the complex material having a three-dimensional structure, a scrap of absorbent cotton was observed in two ways described above. After the pretreatment, the cotton was cut in order to observe both surface and cross section. Figure 2-2(a) shows the SEM images of gold sputtered absorbent cotton. The cross section gave a white

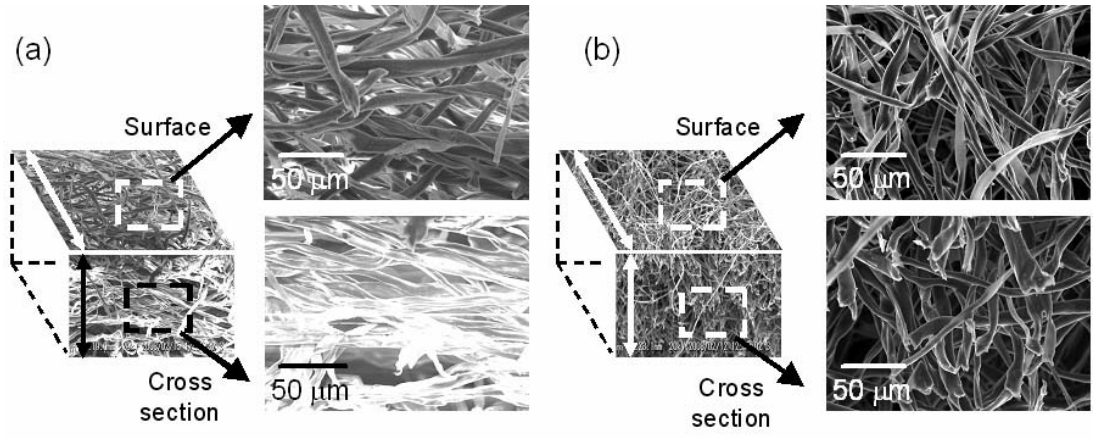

Figure 2-2. SEM images of absorbent cotton pretreated with (a) gold and (b) BMI-TFSA/ethanol solution. The accelerate voltage for SEM observation was 20 kV.

image with lots of noises due to charging although the surface was observed clearly, implying that gold sputtering could not coat the inside of the sample. During sputtering, since gold atoms shot out from the target and ran against the sample, the surface of the sample was coated preferentially. Absorbent cotton soaked in BMI-TFSA diluted by ethanol gave clear images of both surface and cross section without charging, as shown in Figure 2-2(b), because ionic liquid reached inside of the cotton.

2-3-2. Application of ionic liquids for biomaterial

As the next sample, brown seaweed was chosen for SEM observation of the sample wetted by ionic liquid. Brown seaweed is well known to be a Japanese favorite food. It is sold on the market in dry condition. Figure 2-3(a) shows a SEM image of cross section of a dried seaweed leaf whose surface was coated with gold. Volume of the dried seaweed is several times smaller than that of natural one in wet condition. First, it was attempted to swell the dried brown seaweed by putting it in hydrophilic BMI-BF_4 for several hours. Although a little increase in its volume was observed, the magnitude

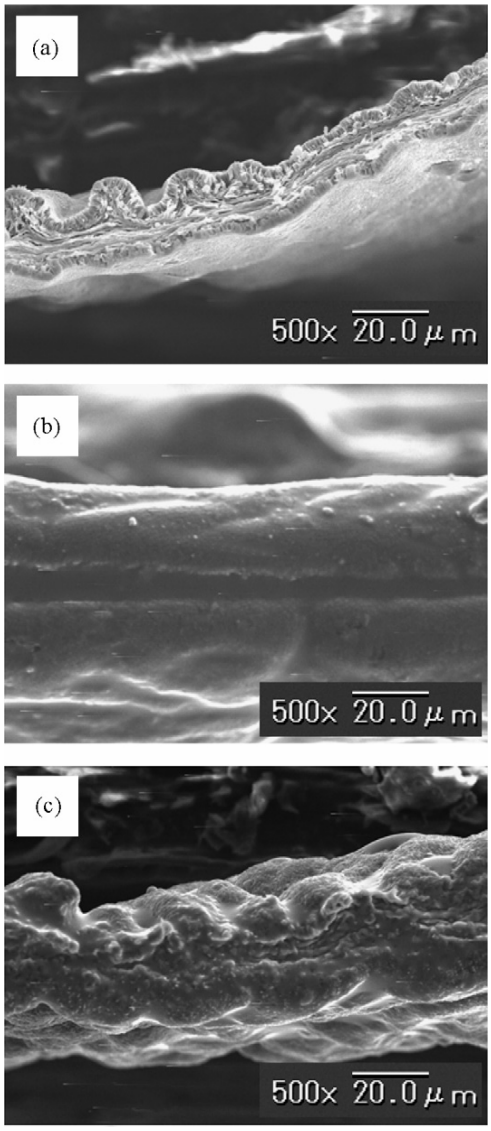

Figure 2-3. SEM images of cross section of a dried seaweed leaf coated with (a) gold and seaweed leaves swollen by water, followed by soaking in (b) BMI-BF_4 and (c) BMI-TFSA under vacuum condition. The accelerate voltage for SEM observation was 20 kV.

of swelling was much smaller than the case of swelling it in water. It was then attempted to make replacement of water contained in swollen seaweed with ionic liquid. A leaf of dried brown seaweed was fully swollen by putting it in water for several minutes. After wiping surface of the swollen seaweed leaf, it was put in a petri dish containing BMI-BF_4. Then, the petri dish was left in an outgassed desiccator for about 2 h to

remove water. Even in vacuum condition, significant volume change of the seaweed in BMI-BF_4 was not recognized, indicating that replacement of water included in the seaweed with ionic liquid was completed. It may be possible that some water molecules were still absorbed on the surface of the seaweed although their presence could not be confirmed in the present study. Figure 2-3(b) is a SEM image of cross section of the resulting seaweed taken after wiping excess amount of ionic liquid on the sample surface. As recognized by comparing it with Figure 2-3(a), the swollen seaweed had a few times larger thickness because of swelling. It is noteworthy that in this case coating of the sample with metal or carbon was not required because ionic liquid in the sample gave electronic conductivity to the sample.

Doing the similar experiments using other ionic liquid clarified that the hydrophilicity of ionic liquid was an important factor. When the swollen seaweed soaked in hydrophobic ionic liquid of BMI-TFSA was put in an outgassed desiccator, significant shrinkage of the seaweed was recognized. Then, it gave a SEM image of partially dried seaweed, as shown in Figure 2-3(c). It is likely that the swollen seaweed having strong affinity to water prevents penetration of hydrophobic ionic liquid in it, resulting in evaporation of water in the sample under vacuum condition. Therefore, use of hydrophilic ionic liquid is essential for replacement of water included in the biomaterial with ionic liquid for its SEM observation.

2-4. Conclusions

It has been clarified that ionic liquids are useful for providing electronic conductivity for insulating materials without any special instrument. In case of samples

showing different morphology in dry and wet states, the use of ionic liquid must be an advanced technique for wet sample observation, evidenced in this chapter by observing a seaweed leaf swollen by ionic liquid. However, this must be applicable to many biological materials if the materials were not got serious damage from ionic liquid. Furthermore, for the samples having three-dimensional structure like absorbent cotton, it is more efficient to use ionic liquid than gold sputtering, in terms of giving electric conductivity inside of the samples.

Chapter 3

Development of In Situ Electrochemical Scanning Electron Microscopy Using Ionic Liquid

3-1. Introduction

In the previous chapters, it was found that ionic liquids could be used as electrolyte solutions for electrochemical reactions (chapter 1) and could be observed by scanning electron microscope (SEM) without charging (chapter 2). These findings suggest the possibility of observing the process of electrochemical phenomena in ionic liquids by SEM. For this purpose, it is necessary to design an appropriate electrochemical cell which could avoid charging by the electron beam irradiation and to build up a new system for electrochemical reaction in the vacuum chamber of the SEM. Redox reaction of polypyrrole (PPy) film was chosen as the first demonstration. It is well known that conducting polymers, such as PPy, polyaniline and polythiophene, exhibit volume changes that accompany their redox reactions because of doping and dedoping of electrolyte ions.[4-8, 97-105] However, since the volume change is slight, it is impossible to conduct direct measurement, even if an optical microscope is used. It has only been estimated by indirect methods, such as actuator tests using a spring electrode entirely covered with the conducting polymer[4, 5, 99, 100] and a bimetal-structured composite film of the conducting polymer and a soft insulating polymer.[6-8, 101-107] In this chapter, I will introduce direct measurements of slight changes in the thickness of a

PPy film with the in situ electrochemical SEM system, modifying a commercially available SEM instrument. I will also show that in situ energy dispersive X-ray fluorescence (EDX) analysis could be employed to detect doping of ions in the polymer and their dedoping.

3-2. Experimental

Ionic liquid of 1-butyl-3-methylimidazolium bis(trifluoromethanesulfonyl)-amide (BMI-TFSA) was pretreated by the same procedure described in chapter 1 before all experiments. Pyrrole (Wako Pure Chemical Ind.) was purified by Kugelrohr distillation. Lithium bis(trifluoromethanesulfonyl) amide (Li-TFSA), lithium tetrafluoroborate (Li-BF_4) and propylene carbonate (Kanto Chemical Co., Inc.) were of regent grade and used without specific purification. Tetrabutylammonium hexafluorophosphate (TBA-PF_6, Aldrich), sodium perchlorate and sodium *p*-toluenesulfonate (Wako Pure Chemical Ind.) were of regent grade and used without specific purification. K-TFSA was prepared by mixing equimolar aqueous solution of KOH and H-TFSA, followed by evaporation and drying in vacuum. The vacuum chamber of the SEM (Keyence VE-8800) was a little modified so as to introduce electric lead wires from a potentiostat (Hokuto Denko, HSV-100). In situ electrochemical SEM measurements were conducted using a glass petri dish (20 mmϕ) containing two Pt electrodes (10 mm × 5.0 mm × 1.0 mm in thickness) and ionic liquid, as an electrochemical cell, as schematically depicted in Figure 3-1. One Pt electrode used as a counter electrode was coated with relatively thick PPy film by electrochemical oxidation of pyrrole solution. Redox reaction of this PPy film allowed occurrence of

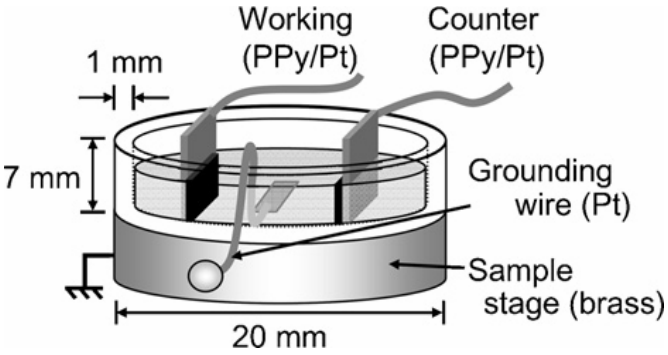

Figure 3-1. Schematic illustration of electrochemical cell for in situ SEM observation of redox reaction of a PPy film deposited on a Pt electrode.

electrochemical reaction on the Pt electrode (a working electrode) without any side reaction. Another Pt foil electrode was also put in the ionic liquid and its other end was connected to the sample stage of the SEM. This worked as a grounding wire and details will be mentioned in Section 3-3-1. Electrochemical reactions were conducted by applying dc voltage between two PPy-deposited Pt electrodes in the vacuum chamber of the SEM. The same electrochemical reaction was conducted out of the vacuum chamber of the SEM using the same electrochemical cell but a reference electrode of Ag/Ag^+ (0.1 M) in BMI-TFSA was put in ionic liquid to measure the net working electrode potential. Thus, the correlation between electrode potential and dc voltage applied between the two Pt electrodes was estimated. A Pt foil electrode and an Ag/Ag^+ (0.1 M) in BMI-TFSA were used as counter and reference electrodes, respectively, for cyclic voltammetry measurements. EDX (EDAX VE-9800) line analysis was conducted using K^+ as a marker reagent in BMI-TFSA including 100 mM K-TFSA. The measurements were carried out by drawing intensity of the energy band at 3.310 keV with dead times around 30 %.

3-3. Results and Discussion

3-3-1. Fabrication of the in situ electrochemical SEM system

Figure 3-1 shows a schematic illustration of the cell used for in situ electrochemical SEM observation. It was composed of a glass petri dish, two Pt plate electrodes and another Pt foil electrode. Although it would be better to use a metallic cell considering the electrical conduction between the BMI-TFSA in the cell and the sample stage, it would be very difficult to prevent the electrodes from touching the cell, as the sample stage is so small. When the cell was put on a sample stage of the SEM, an end of the Pt foil electrode was touched to the sample stage by a screw for making electronic contact between ionic liquid in the cell and the sample stage. The role of this grounding wire could be clearly recognized from the SEM images of ionic liquid in the

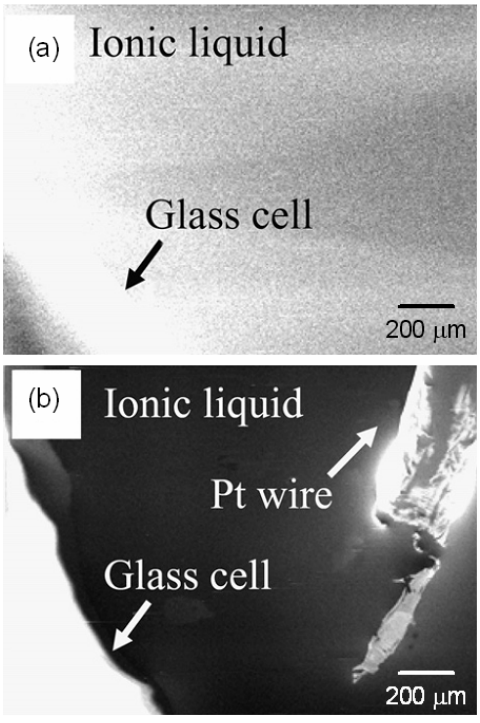

Figure 3-2. SEM images of a part of a glass cell and ionic liquid in the cell in (a) the absence and (b) the presence of a Pt wire connecting ionic liquid and a sample stage. The accelerate voltage for SEM observation was 20 kV.

glass cell, as shown in Figure 3-2. When the cell was observed without the grounding wire, the insulating glass cell and ionic liquid in the cell were charged, giving a bright image, as shown in Figure 3-2(a). However, charges in the ionic liquid were effectively removed when the grounding Pt wire was set in the cell, as shown in Figure 3-2(b). Unfortunately, it has not been clarified how the irradiated electrons behave in ionic liquid but electrons in ionic liquid have been studied by fast pulse radiolysis experiments using methyltributylammonium-TFSA[29] and XPS measurement.[37-41] The former technique generated solvated electrons having a life time of 300 ns when 8.7 MeV electron pulse were injected. It is then speculated that generation of the solvated electrons occurs also in the case of SEM observation, allowing ionic liquid to behave like an electronic conducting material. However, it should be considered that any chemical reaction including decomposition of ionic liquid takes place although total electron dose irradiated to ionic liquid in the SEM observation is usually quite small as compared to the amount of ionic liquid. Clarification of this possibility has been the next subject.

The electrochemical cell shown in Figure 3-1 was used for observation of redox reaction of PPy. In this case, the vertically set electrode was observed from topside, giving an image of cross section of the electrode, as shown in Figure 3-3. The PPy film was prepared by electrochemical oxidation at 0.4 mA cm^{-2} in propylene carbonate containing 0.06 M pyrrole and 0.05 M TBA-PF_6 for 20 min. From this SEM image, the film thickness is estimated to be 30 ± 3 μm. The electrode was soaked in ionic liquid but small top portion was exposed from the ionic liquid, allowing observation of the electrode cross section without interference by the ionic liquid, although this is not evident in Figure 3-3.

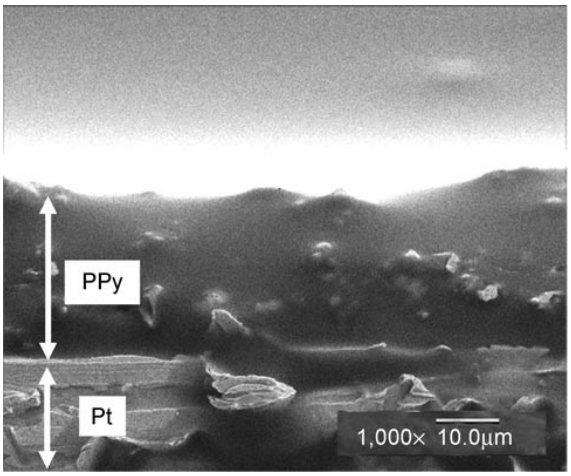

Figure 3-3. SEM image of a cross section of PPy deposited on the Pt working electrode immersed in BMI-TFSA. The acceleration voltage for SEM observation was 20 kV.

3-3-2. In situ electrochemical SEM observation of PPy film

Although attempts were made to observe changes in the film thickness at this magnification, these changes were insufficient to recognize in the image (Figure 3-3). Then, a section of the PPy surface was observed at a higher magnification and the SEM images were taken by changing applied dc voltage. As already mentioned in the experimental section, the Pt electrode used as a counter electrode was coated with PPy exhibiting redox reaction. Since relatively large amount of PPy was deposited, redox reaction of PPy alone should take place as counter reaction of the working electrode reaction, allowing occurrence of electrochemical reactions without any unexpected side reaction in the vacuum chamber of the SEM. The obtained images are arrayed in Figure 3-4 for comparison of the PPy surface level at each applied voltage. The numbers given under the SEM images in Figure 3-4 indicate the electrode potentials applied to the working electrode with respect to Ag/Ag^+ (0.1 M) in BMI-TFSA. The initial dc voltage was –2.5 V, which polarized the working electrode at –1.7 V vs. Ag/Ag^+ (0.1 M), and

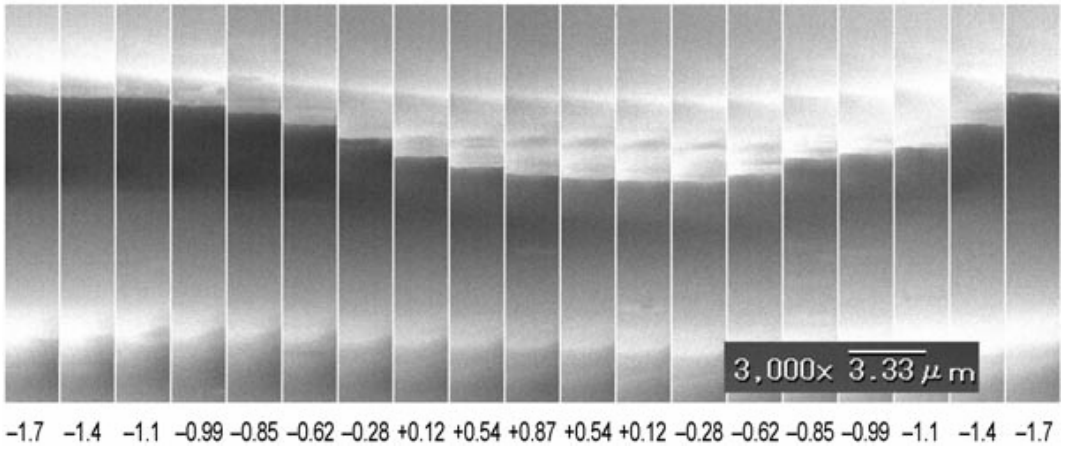

Figure 3-4. In situ electrochemical SEM observation of surface level changes of a PPy film in BMI-TFSA caused by changing electrode potential. The working electrode potentials were indicated referring to Ag/Ag^+. The acceleration voltage for SEM observation was 20 kV.

the voltage was increased to 2.0 V at intervals of 0.5 V. Each voltage was applied for several tens of seconds until the current had decreased to less than 1.0 μA cm^{-2}. Figure 3-4 shows that the PPy surface level sinks with positive potential shifts, implying a decrease in the film thickness. An image drift does not occur when the applied dc voltage was changed, since no level change was observed when a PPy/Pt interface was investigated under the same conditions.

Figure 3-5 shows a typical cyclic voltammogram of a PPy film-coated Pt electrode taken at a scan rate of 0.05 V s^{-1} in BMI-TFSA (——). The PPy film was prepared under the same conditions as those used for preparation of the PPy film subjected to the in situ electrochemical SEM observation. A Pt foil electrode and an Ag/Ag^+ (0.1 M) in BMI-TFSA were used as counter and reference electrodes, respectively. Oxidation and reduction waves are seen in the voltammogram, indicating that redox reaction of the PPy film accompanying doping and dedoping of ionic species definitely took place in BMI-TFSA. In the same figure, the film thickness as a function

of electrode potential estimated from the results shown in Figure 3-4 are also plotted (-----). The relationship between the PPy film thickness changes and the sum of charges in negative potential shift estimated by integrating cathodic currents observed in Figure 3-5 is plotted in Figure 3-6, showing a linear relationship. The same relationship is seen during the oxidation of PPy though not shown here. The linear relationship shows that the amount of charge on PPy is directly proportional to the magnitude of the change in film thickness.

Several reports on the redox reactions of conducting polymers have been published.[4-8, 103, 104] For PPy, two modes of redox reaction have been reported; reactions accompanying doping and dedoping of anions and of cations. In the latter case, anions are immobilized in the polymer as fixed dopants, resulting in doping of cations by reduction of positively charged PPy to neutral PPy. The results of decrease in the PPy film thickness by its oxidation shown in Figure 3-5 strongly suggest that this redox reaction corresponds to the reaction mode accompanying movement of cations.

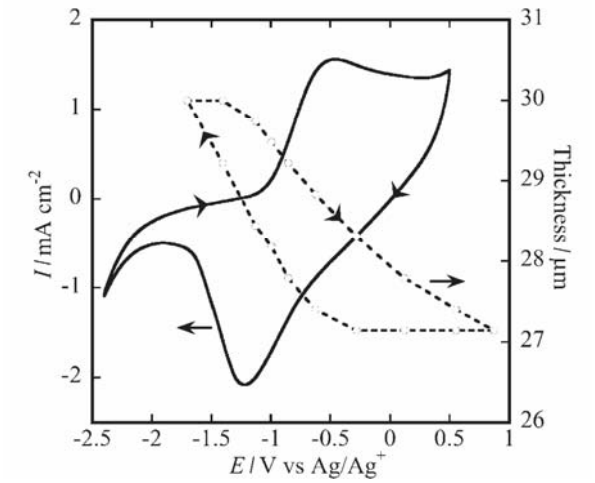

Figure 3-5. Cyclic voltammogram of PPy film-coated Pt electrode taken at a scan rate of 0.05 V s^{-1} (solid line) and changes in thickness of the film as a function of electrode potential (broken line).

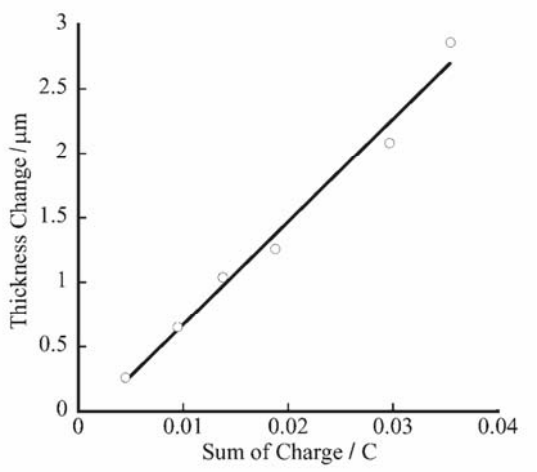

Figure 3-6. Relationship between thickness change and sum of charge during reduction of PPy film.

The PPy films prepared under different conditions were also subjected to the in situ electrochemical SEM observation. The preparation conditions of PPy films and results obtained by their in situ SEM observations are summarized in Table 3-1. Contrary to the result mentioned above, the PPy film prepared in aqueous solution containing sodium *p*-toluenesulfonate (*p*-TSNa) exhibited an increase in the film thickness by oxidation. In this case, *p*-toluenesulfonate anion that should be doped in the freshly prepared PPy film can be eliminated by reduction of the film, and doping and dedoping of anion of the ionic liquid, i.e. $TFSA^-$ are accompanied by the successive redox reaction. The PPy films prepared from nonaqueous solutions seem to take the reaction mode of cation doping and dedoping, as judged from the results of an increase

Table 3-1. Changes in thickness of PPy film prepared under different conditions.

Polymerization conditions				In situ measurement		
Electrolyte[a] solution	Current density ($mA\ cm^{-2}$)	Time (min)	Thickness of oxidized film (μm)	Electrolyte solution	Thickness change by reduction (μm)	Rate (%)
p-TSNa/H_2O	0.4	20	40	BMI- TFSA	−0.6	−1.5
p-TSNa/H_2O	20	60	400	BMI- TFSA	−4.0	−1.0
Li-TFSA/AN	0.4	20	25	BMI- TFSA	+2.5	+10
Li-BF_4/AN	0.4	20	40	BMI-BF_4	+10	+25
TBA-PF_6/PC	0.4	20	30	BMI- TFSA	+3.9	+13

[a] AN, acetonitrile; PC, propyrene carbonate; *p*-TSNa, sodium *p*-toluenesulfonate.

in their film thicknesses by reduction. The rates of film thickness changes obtained for the latter reaction mode are significantly larger than those for the former reaction mode, suggesting that the reaction mode accompanying doping and dedoping of electrolyte cation is more desirable to fabricate actuators.

3-3-3. In situ EDX measurement

The in situ electrochemical SEM observation has a possibility to conduct analysis of the composition changes of the specimen under polarization conditions using EDX attached to the SEM. This kind of measurement could potentially be used for clarifying the reaction mechanisms. Then, it was attempted to confirm the reaction mechanism mentioned in Figure 3-4, if the PPy indeed undergoes reduction by the movement of cations. However, since a BMI cation is composed of carbon, hydrogen and nitrogen, as is PPy, it seemed to be difficult to distinguish the cations in PPy by EDX. Therefore, potassium bis(trifluoromethanesulfonyl)amide (K-TFSA) was dissolved in BMI-TFSA in order to use K^+ as a marker for EDX analysis. In this ionic liquid, doping and dedoping of K^+ and BMI^+ should take place simultaneously.

The EDX line analysis was conducted along a line drawn from the ionic liquid to PPy film by measuring K-Kα X-ray intensities at 3.310 keV with the acceleration voltage of 20 kV. As shown in Figure 3-7, the EDX measurements could be conducted without any problem even under polarization conditions. The X-ray intensities of K-Kα in PPy polarized at –1.70 V vs. Ag/Ag^+ were much larger than those in the film polarized at 0.87 V vs. Ag/Ag^+, while no significant difference in the K-Kα X-ray intensities was observed in the ionic liquid. These results clearly indicate doping of K^+ into the PPy film upon reduction and dedoping of K^+ into the PPy film upon oxidation.

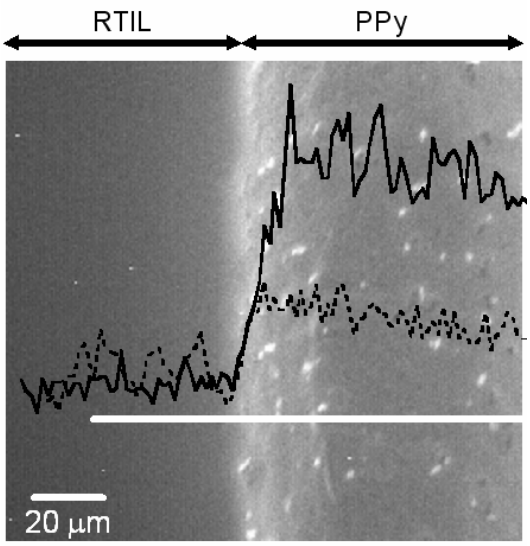

Figure 3-7. EDX line analysis of K^+ along a white line drawn in the SEM image by K-Kα X-ray intensities at 3.310 keV. Results obtained for PPy polarized at –1.70 (solid line) and +0.87 V vs. Ag/Ag^+ (broken line) are shown. The acceleration voltage for SEM observation was 20 kV.

Although not shown here, the EDX line analysis was also done on S-Kα X-ray intensities at 2.308 keV to gauge the change in the amount of $TFSA^-$ in PPy. No significant difference in the S intensity was observed upon reduction of PPy, evidencing clearly that $TFSA^-$ stayed in the polymer as a fixed dopant. Based on the EDX measurements and the results shown in Figure 3-6, it can be concluded that only the doping and dedoping of cations exclusively cause the changes in the PPy film.

3-4. Conclusions

An in situ electrochemical SEM system which allows a specimen to be observed under polarization conditions has been developed. The use of ionic liquids as electrolyte enabled this measurement. The observation of a PPy film polarized at various potentials clearly revealed that its oxidation and reduction were accompanied by

decrease and increases, respectively, in the film thickness. It was subsequently confirmed by EDX measurement under polarization conditions that doping of cations into the PPy film took place upon reduction and dedoping of cations from the film occurs upon oxidation.

Commercially available SEM instruments, including those utilized here are designed to provide magnified still images. However, they have a viewing mode that allows the viewing of samples in real time in order to determine an appropriate position for obtaining the final still image. In the present study, I recognized changes in the PPy film thickness in real time when the polarizing potential was changed, although the film thickness at each potential was measured from each still image (Figure 3-4). Investigation to consider the moving image in the viewing mode at a sufficiently fast rate is underway.

Chapter 4

In Situ Scanning Electron Microscope Observation of Metal Deposition from Ionic Liquids

4-1. Introduction

In the kinetic studies on metal deposition, observation of the deposited metal surfaces with scanning electron microscope (SEM) gives information on morphology of the deposited metal, from which growth mechanisms can be speculated. However, it is required to prepare multiple samples with different deposition time for SEM observations in order to know changes in the morphology as a function of deposition time. In other words, a requirement of vacuum condition limits SEM to ex situ observation. In situ observations of metal deposition with high magnification have used to be mainly conducted by the scanning probe microscopes including scanning tunneling microscope and atomic force microscope.[108-110] Based on the finding described in previous chapters; metal electrodeposition (chapter 1) and in situ electrochemical SEM observation using ionic liquids (chapter 3), it would be possible to observe the process of metal deposition in real time.

In this chapter, I will describe a new electrochemical system, which allows in situ SEM observation of metal deposition from ionic liquid. If a conventional cell were used, ionic liquid in the cell should disturb observation of metal deposition on the electrode surface. A specific cell which is appropriate for observing morphology

changes in real time is designed. Using it, SEM observation of silver electrodeposition from ionic liquid containing silver ions will be demonstrated.

4-2. Experimental

1-butyl-3-methylimidazolium bis(trifluoromethanesulfonyl)amide (BMI-TFSA, Kanto Chemical Co., Inc.) was purified by the same way described in chapter 1. Silver bis(trifluoromethanesulfonyl)amide (Ag-TFSA) was prepared by mixing Ag_2O and H-TFSA in a molar ration of 1:2, followed by evaporation and drying in vacuum.[111] The SEM (Keyence VE-8800) equipped with energy dispersive X-ray fluorescence (EDX, EDAX VE-9800) was a little modified to introduce electric lead wires from a potentiostat (Hokuto Denko, HSV-100).

4-3. Results and Discussion

4-3-1. Quasi in situ observation using conventional electrochemical cell

Figure 4-1 shows cyclic voltammogram of a Pt wire electrode taken in BMI-TFSA containing 20 mM Ag-TFSA at 0.02 V s^{-1}. A cathodic wave due to Ag deposition and an anodic wave due to stripping of the deposited Ag were clearly seen at around –0.22 and 0.02 V, respectively.

For the SEM observation, the working electrode was horizontally positioned just under the ionic liquid surface. However, since the ionic liquid presenting on the electrode surface made resolution of the SEM image a little lower, reaction was intermitted and the electrode surface was exposed from ionic liquid during taking a SEM image. In this respect, this technique cannot be regarded as a proper real time

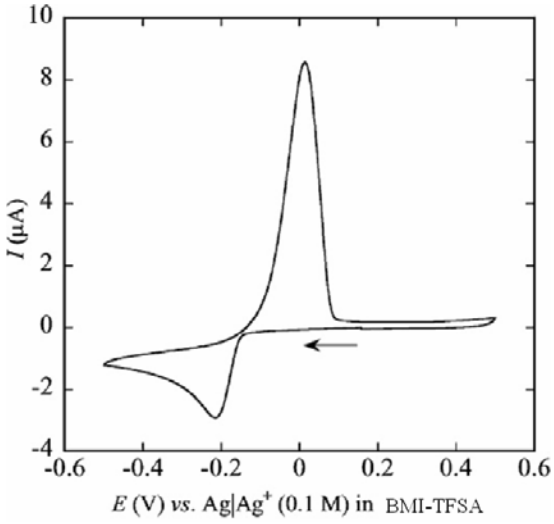

Figure 4-1. Cyclic voltammogram of Pt electrode taken at 0.02 Vs^{-1} in BMI-TFSA containing 20 mM Ag-TFSA.

observation. The exposure of the electrode surface was conducted by tilting the sample stage a little. Silver deposition was made by polarizing the electrode at –0.5 V vs. Ag/Ag^+ (0.1 M) in BMI-TFSA containing silver ion. Figure 4-2(b) shows the SEM image obtained after Ag deposition for 35 min. Comparison of this with the SEM image before deposition shown in Figure 4-2(a) revealed that the electrode surface was entirely covered with Ag layer, on which some Ag particles appeared. After deposition, the applied potential was changed to 0.5 V to induce oxidative dissolution of the deposited Ag, giving the SEM image shown in Figure 4-2(c), which is identical with the Pt surface before Ag deposition (Figure 4-2(a)).

The possibility to employ EDX analysis for the electrode polarized in ionic liquid was examined using this Ag-deposited Pt electrode. The EDX spectra shown by broken line and solid line in Figure 4-3 were taken for the SEM images as shown in Figure 4-2(a) and (b), respectively. The X-ray band due to Pt-Mα at 2.054 keV was

found in both electrodes and the band due to Ag-Lα at 2.982 keV appeared after deposition. The shape of the spectra was not influenced at all even under polarization condition. If Ag deposition and its oxidative dissolution were induced during measurements, changes in the intensity of the Ag-Lα band were recognized.

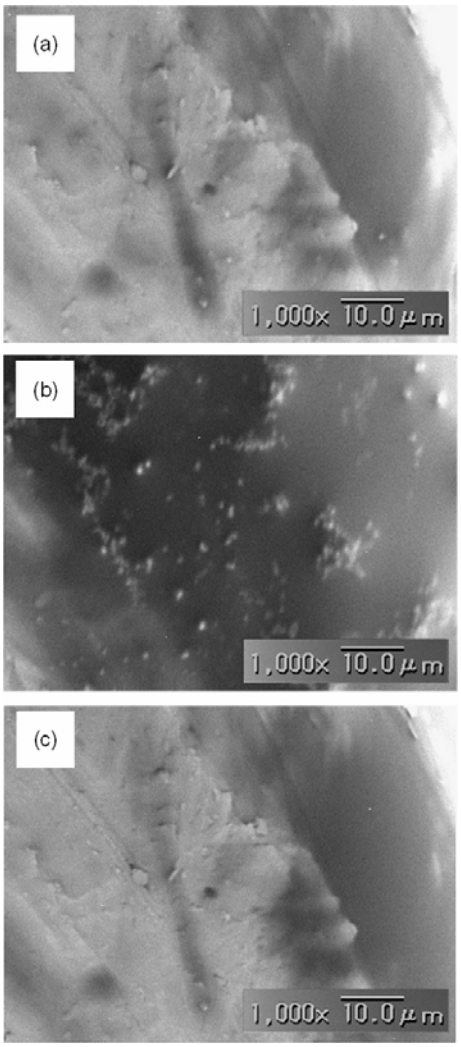

Figure 4-2. SEM images of a Pt electrode (a) before and (b) after in situ electrochemical deposition of Ag and (c) an image of the same electrode taken after oxidative dissolution of deposited Ag. The accelerate voltage for SEM observation was 10 kV.

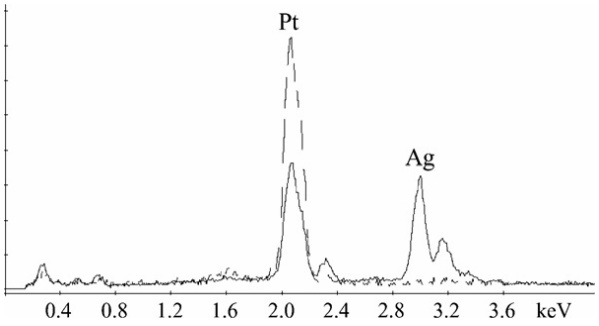

Figure 4-3. EDX spectra of Pt electrode before (broken line) and after (solid line) electrochemical Ag deposition.

4-3-2. Designing a specific cell for metal electrodeposition

Electrodeposition of metal takes place on an electrode surface which contacts with electrolyte solution. It is necessary to consider the disturbance by ionic liquid in order to observe electrochemical reactions in ionic liquid by SEM. One of ways to avoid it may be fabrication of an electrochemical cell, which allows occurrence of electrochemical reactions at very shallow area underneath the surface of ionic liquid. For this purpose, a fluorine doped tin oxide-coated glass (FTO-glass; Asahi Glass Co., Ltd.) having an FTO layer of 0.9 μm with sheet resistance of 10 Ω/□, was used to fabricate an electrochemical cell, as schematically shown in Figure 4-4. Two grooves having T-shape were cut on its oxide layer to be divided into three regions which were used as working, counter, and grounding electrodes, respectively. A Pt wire was attached to each part with an electrically conducting carbon adhesion tape. Small amount of BMI-TFSA containing 20 mM Ag-TFSA was carefully put in the groove between working and counter electrodes without its overflow on the working electrode surface. Some amount of ionic liquid was spread on the grounding electrode surface which is electrically contacted with the sample stage. This can easily be conducted because wettability of the FTO surface to BMI-TFSA is quite high.

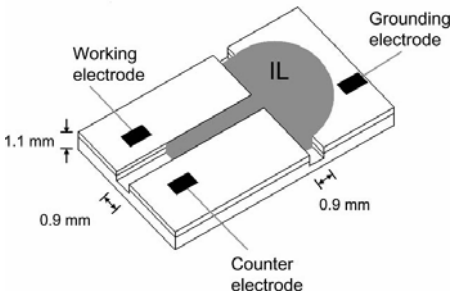

Figure 4-4. Schematic illustration of electrochemical cell fabricated by cutting grooves on an FTO-glass for in situ SEM observation of electrochemical reactions.

Cyclic voltammetry was conducted in the standard ambient condition at 0.05 V s^{-1} using this electrochemical cell with a reference electrode of Ag/Ag^{+} (0.1 M) in BMI-TFSA put in the ionic liquid. Prior to measurements, silver metal was deposited on the counter electrode by passing constant current (2 μA) for 3 min between the counter electrode and an Ag wire which touched to the ionic liquid in the groove. The deposited Ag allowed occurrence of electrochemical reaction at the working electrode without any unexpected side reaction. The obtained voltammogram was shown in Figure 4-5.

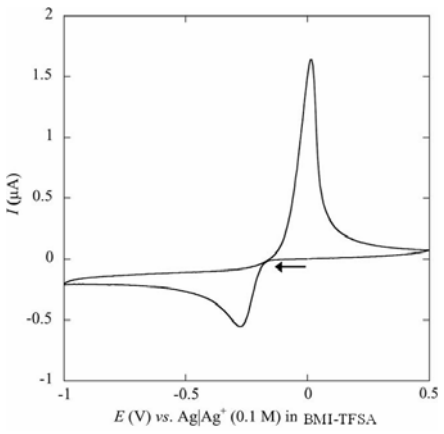

Figure 4-5. Cyclic voltammogram of BMI-TFSA containing 20 mM Ag-TFSA taken by the FTO-glass electrochemical cell at 0.05 V s^{-1}.

Cathodic and anodic wave are seen at around –0.31 and +0.04 V, respectively. The obtained CV shape was quite similar to the CV shape obtained using the FTO glass surface as a working electrode. These results imply that both cross section and surface of the FTO layer possess the same characteristic as an electrode.

4-3-3. Comparison of electrochemical behavior with growth of metal deposition

In situ SEM observation of silver deposition was made by applying electrode

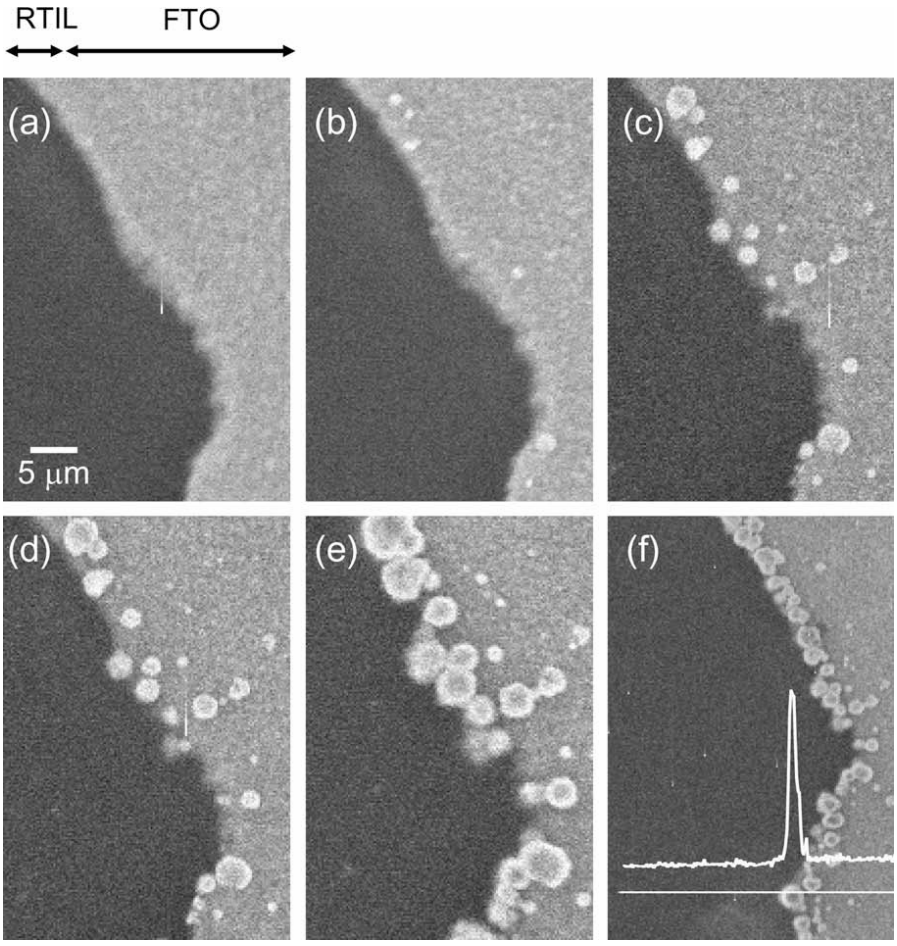

Figure 4-6. SEM images of gradual deposition of silver particles polarized at –0.22 V vs. Ag/Ag^+ for (a) 0, (b) 15, (c) 30, (d) 60, (e) 180 min and (f) EDX line analysis of Ag along a white line drawn in the SEM image by Ag-Lα X-ray intensities at 2.982 keV. The accelerating voltage for SEM observation was 20 kV.

potential to the working electrode, while observing the edge of FTO layer. The polarization potential chosen was –0.22 V, which was a little more negative than the onset potential of silver deposition (–0.15 V). It is known that silver deposition with nucleus growth is dominant in ionic liquid at such the polarization potentials.[112-114] As shown in Figure 4-6, it was succeeded to observe gradual growth of silver on the FTO electrode. Polarization for 15 min generated granular deposits (Figure 4-6(b)), followed by increase in number of Ag particles and their growth. After the in situ observation, EDX line analysis was carried out by detection of X-ray band derived from Ag-Lα at 2.982 keV along a white line drawn from ionic liquid to the FTO in Figure 4-6(f). The X-ray intensity became large in the region where deposited particle was seen, confirming that the particles were certainly Ag particles.

Similar experiment was conducted but the applied potential was shifted to –1.14 V vs. Ag/Ag^+ where the reaction rate is determined by diffusion of Ag^+, as judged from the voltammogram shown in Figure 4-5. In such the reaction condition, several metals including Ag and Cu tend to form aciculate deposits.[114-116] These phenomena could be explained on the fact that the diffusion of Ag^+ to the end of the branch would prefer to the electrode substrate, leading the further growth of deposited dendrites. As a matter of fact, the in situ SEM observation gave clear SEM images showing gradual growth of Ag dendrites, as shown in Figure 4-7(b-e). EDX analysis revealed again that the obtained dendrites were Ag, as shown in Figure 4-7(f). It is impossible to take such the sequential SEM images of growth of one dendrite by the usual ex situ SEM observation.

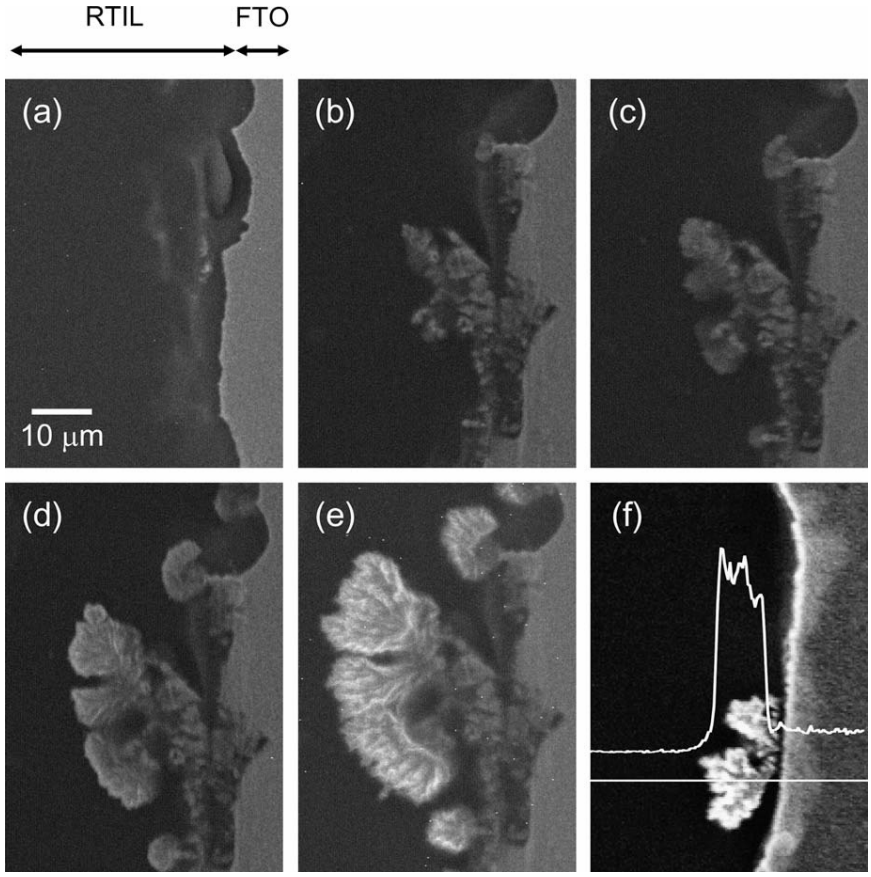

Figure 4-7. SEM images of gradual generation of silver dendrite polarized at –1.14 V vs. Ag/Ag^+ for (a) 0, (b) 15, (c) 30, (d) 60, (e) 180 min and (f) EDX line analysis of Ag along a white line drawn in the SEM image by Ag-Lα X-ray intensities at 2.982 keV. The accelerating voltage for SEM observation was 20 kV.

4-4. Conclusions

The results reveal the development of in situ SEM observation system for metal electrodeposition. The fabricated system allowed to find out difference in the morphology of Ag deposited at different electrode potential and sequential growth of the deposited metal, using an FTO glass plate. However, based on the results, similar electrochemical cells were fabricated using slide glasses that were coated with Pt, Au,

and other metals by a sputtering method. It was then found that those metal-deposited glasses, on which grooves were cut, worked well for in situ SEM observation of electrochemical metal deposition, implying that the method developed here has been widely applicable to in situ SEM observation of several kinds of electrochemical reactions.

Summary

Ionic liquids could be used as electrolyte solution without solvent for electrochemical desorption of *n*-alkanethiol self-assembled monolayer and electrodeposition of aluminum alloys. Their electrochemical behaviors were different from those in conventional aqueous solutions. In addition, ionic liquids behaved as antistatic agents of insulating materials for electron microscopy. This fact was easily applied to biomaterials including much water such as seaweed.

During implementation of the in situ observation, it was found that SEM observation of the PPy film polarized in ionic liquid could be conducted for long time without giving any damage to the SEM instrument or the specimen. Such the favourable situations are owed to ionic liquid possessing negligible vapour pressure in room temperature and antistatic property. Even if ionic liquid is put in an insulating vessel, its SEM observation is possible by connecting ionic liquid to a metal sample stage with a grounding Pt wire. It was confirmed that EDX analysis was also available even under polarization conditions. The combination of in situ SEM observation and EDX analysis must be a powerful method to clarify reaction mechanisms of the electrochemically active materials.

In situ SEM observation is appropriate for observing non-ordered morphology of materials. For example, since the images of the growth of metal particles (Figure 4-6) showed no change in electrode surface but cross section view of the deposited Ag floating on ionic liquid, it is impossible to observe them by the scanning probe microscopes.

Accordingly, the in situ electrochemical SEM technique developed in the present study must be widely applicable to not only electrochemical reactions but also other chemical phenomena, including various chemical and biochemical reactions. Further investigation aiming development of other in situ measurement systems and clarification of phenomena whose mechanisms are unknown by using the developed systems are currently in progress.

List of Publications

1. Electrochemical desorption of a self-assembled monolayer of alkanethiol in ionic liquids

   Daisuke Oyamatsu, Takeshi Fujita, Satoshi Arimoto, Hirokazu Munakata, Hajime Matsumoto and Susumu Kuwabata

   Journal of Electroanalytical Chemistry, 2008, 615, 110-116.

2. Electrodeposition of Al-Mo-Ti Ternary Alloys in the Lewis Acidic Aluminum Chloride–1-Ethyl-3-methylimidazolium Chloride Room-Temperature Ionic Liquid

   Tetsuya Tsuda, Satoshi Arimoto, Susumu Kuwabata and Charles L. Hussey

   Journal of The Electrochemical Society, 2008, 155(4), D256-D262.

3. Development of In Situ Electrochemical Scanning Electron Microscopy with Ionic Liquids as Electrolytes

   Satoshi Arimoto, Daisuke Oyamatsu, Tsukasa Torimoto and Susumu Kuwabata

   ChemPhysChem, 2008, 9(5), 763-767.

4. Development of new techniques for scanning electron microscope observation using ionic liquid

   Satoshi Arimoto, Masaharu Sugimura, Hitoshi Kageyama, Tsukasa Torimoto and Susumu Kuwabata

   Electrochimica Acta, 2008, 53, 6228-6234.

5. Development of in situ scanning electron microscope system for real time observation of metal deposition from ionic liquid

   Satoshi Arimoto, Hitoshi Kageyama, Tsukasa Torimoto and Susumu Kuwabata

   Electrochemistry Communications, 2008, 10, 1901-1904.

Supplementary Publication

1. Electrocatalytic Activity of Pt and Ru Photodeposited Polyaniline Electrodes for Methanol Oxidation

   Satoshi Arimoto, Hiroyuki Nakano, Takeshi Fujita, Yasuhiro Tachibana and Susumu Kuwabata

   Electrochemistry, 2007, 75(1), 39-44.

Acknowledgements

First of all, I would like to express my great appreciation and gratitude to Professor Dr. Susumu Kuwabata at Department of Applied Chemistry, Graduate School of Engineering, Osaka University for his continuous guidance, invaluable suggestions and encouragement throughout the course of this work. I am also grateful to Professor Dr. Seiichi Tagawa and Professor Dr. Hiroshi Uyama for reviewing this thesis and their helpful advice. I am obliged to Dr. Yasuhiro Tachibana, Dr. Tetsuya Tsuda, Dr. Eiko Mochizuki and Dr. Daisuke Oyamatsu for their sincere encouragement and useful advice. I also would like to thank Professor Dr. Charles L. Hussey at The University of Mississippi and Professor Dr. Tsukasa Torimoto at Nagoya University for their expert comments for performing experiments.

I appreciate all members in Applied Electrochemistry Laboratory, especially my co-workers, Dr. Hiroyuki Nakano, Mr. Takeshi Fujita, Mr. Masaharu Sugimura, Mr. Hiroshi Tenmyo, Mr. Hitoshi Kageyama, Mr. Takasuke Kurihara, Mr. Yuichi Sato, Mr. Kosuke Inoue, Mr. Satoshi Makuta, Mr. Koshiro Kondo and Mr. Yasunori Hoshino whose efforts enabled to progress this work.

Finally, I wish to express my deepest gratitude to my parents, Toshio Arimoto and Yasuko Arimoto, and my younger brother, Yuji Arimoto for their hearty encouragements and supports.

Satoshi Arimoto

March, 2009

References

[1] P. Bonhôte, A.-P. Dias, N. Papageorgiou, K. Kalyanasundaram and M. Gräzel, *Inorg. Chem.* **1996**, 35, 1168.

[2] V. R. Koch, C. Nanjundiah, G. B. Appetecchi and B. Scrosati, *J. Electrochem. Soc.* **1995**, 142, L116.

[3] S.-Y. Lee, H. H. Yong, Y. J. Lee, S. K. Kim and S. Ahn, *J. Phys. Chem. B.* **2005**, 109, 13663.

[4] J. Ding, L. Liu, G. M. Spinks, D. Zhou, G. G. Wallace and J. Gillespie, *Synth. Met.* **2003**, 138, 391.

[5] J. Ding, D. Zhou, G. Spinks, G. Wallace, S. Forsyth, M. Forsyth and D. MacFarlane, *Chem. Mater.* **2003**, 15, 2392.

[6] F. Vidal, C. Plesse, D. Teyssié and C. Chevrot, *Synth. Met.* **2004**, 142, 287.

[7] D. Zhou, G. M. Spinks, G. G. Wallace, C. Tiyapiboonchaiya, D. R. MacFarlane, M. Forsyth and J. Sun, *Electrochim. Acta*. **2003**, 48, 2355.

[8] W. Lu, A. G. Fadeev, B. Qi, E. Smela, B. R. Mattes, J. Ding, G. M. Spinks, J. Mazurkiewicz, D. Zhou, G. G. Wallace, D. R. Macfarlane, S. A. Forsyth and M. Forsyth, *Science*. **2002**, 297, 983.

[9] H. Matsumoto, T. Matsuda, T. Tsuda, R. Hagiwara, Y. Ito and Y. Miyazaki, *Chem. Lett.* **2001**, 26.

[10] H. Matsumoto, H. Sakaebe and K. Tatsumi, *J. Power Source*. **2005**, 146, 45.

[11] H. Nakamoto, A. Noda, K. Hayamizu, S. Hayashi, H. Hamaguchi and M. Watanabe, *J. Phys. Chem. C*. **2007**, 111, 1541.

[12] A. Noda, M. A. B. H. Susan, K. Kudo, S. Mitsushima, K. Hayamizu and M. Watanabe, *J. Phys. Chem. B.* **2003**, 107, 4024.

[13] N. Papageorgiou, Y. Athanassov, M. Armand, P. Bonhôte, H. Pettersson, A. Azam and M. Grätzel, *J. Electrochem. Soc.* **1996**, 143, 3099.

[14] H. Sakaebe and H. Matsumoto, *Electrochem. Commun.* **2003**, 5, 594.

[15] S. Seki, Y. Kobayashi, H. Miyashiro, Y. Ohno, A. Usami, Y. Mita, N. Kihira, M. Watanabe and N. Terada, *J. Phys. Chem. B*. **2006**, 110, 10228.

[16] S. Seki, Y. Kobayashi, H. Miyashiro, Y. Ohno, A. Usami, Y. Mita, M. Watanabe and N. Terada, *Chem. Commun.* **2006**, 544.

[17] R. F. Souza, J. C. Padilha, R. S. Gonçalves and J. Dupont, *Electrochem. Commun.* **2003**, 5, 728.

[18] T. Schubert, S. Z. E. Abedin, A. P. Abbott, K. J. McKenzie, K. S. Ryder and F. Endres, *Electrodeposition of Metals, in: F. Endres,* A. P. Abbott, and D. R. MacFarlane (Eds.), *Electrodeposition from Ionic Liquids*, Wiley-VCH, pp.83-123. **2008**.

[19] F. H. Hurley and T. P. Wier, *J. Electrochem. Soc.* **1951**, 98, 203.

[20] J. S. Wilkes and M. J. Zaworotko, *J. Chem. Soc., Chem. Commun.* **1992**, 965.

[21] E. Eycken, P. Appukkuttan, W. D. Borggraeve, W. Dehaen, D. Dallinger and C. O. Kappe, *J. Org. Chem.* **2002**, 67, 7904.

[22] K. Fukumoto and H. Ohno, *Angew. Chem. Int. Ed.* **2007**, 46, 1852.

[23] C. Hubert, J. L. Renaud, B. Demerseman, C. Fischmeister and C. Bruneau, *J. Mol. Catal. A: Chem.* **2005**, 237, 161.

[24] Y. R. Jorapur and D. Y. Chi, *J. Org. Chem.* **2005**, 70, 10774.

[25] J. Mo, L. Xu and J. Xiao, *J. Am. Chem. Soc.* **2005**, 127, 751.

[26] E. Naudin, H. A. Ho, S. Branchaud, L. Breau and D. Bélanger, *J. Phys. Chem. B*. **2002**, 106, 10585.

[27] J. Ross, W. Chen, L. Xu and J. Xiao, *Organometallics*. **2001**, 20, 138.

[28] T. Welton, *Chem. Rev.* **1999**, 99, 2071.

[29] J. F. Wishart and P. Neta, *J. Phys. Chem. B*. **2003**, 107, 7261.

[30] C. Zhong, T. Sasaki, M. Tada and Y. Iwasawa, *J. Catal.* **2006**, 242, 357.

[31] M. J. Earle, J. M. S. S. Esperança, M. A. Gilea, J. N. C. Lopes, L. P. N. Rebelo, J. W. Magee, K. R. Seddon and J. A. Widegren, *Nature*. **2006**, 439, 831.

[32] J. P. Armstrong, C. Hurst, R. G. Jones, P. Licence, K. R. J. Lovelock, C. J. Satterley and I. J.V-Garcia, *Phys. Chem. Chem. Phys.* **2007**, 9, 982.

[33] J. O. Valderrama and P. A. Robels, *Ind. Eng. Chem. Res.* **2007**, 46, 1338.

[34] S. Kuwabata, A. Kongkanand, D. Oyamatsu and T. Torimoto, *Chem. Lett.* **2006**, 35, 600.

[35] K. Okazaki, T. Kiyama, K. Hirahara, N. Tanaka, S. Kuwabata and T. Torimoto, *Chem. Commun.* **2008**, 691.

[36] T. Torimoto, K. Okazaki, T. Kiyama, K. Hirahara, N. Tanaka and S. Kuwabata, *Appl. Phys. Lett.* **2006**, 89, 243117.

[37] C. Aliaga, C. S. Santos and S. Baldelli, *Phys. Chem. Chem. Phys.* **2007**, 9, 3683.

[38] O. Höfft, S. Bahr, M. Himmerlich, S. Krischok, J. A. Schaefer and V. Kempter, *Langmuir*. **2006**, 22, 7120.

[39] S. Krischok, M. Eremtchenko, M. Himmerlich, P. Lorenz, J. Uhlig, A. Neumann, R. Öttking, W. J. D. Beenken, O. Höfft, S. Bahr, V. Kempter and J. A. Schaefer, *J. Phys. Chem. B*. **2007**, 111, 4801.

[40] E. M. Smith, I. J. V. Garcia, D. Briggs and P. Licence, *Chem. Commun.* **2005**, 5633.

[41] E. F. Smith, F. J. M. Rutten, I. J. V-Garcia, D. Briggs and P. Licence, *Langmuir*. **2006**, 22, 9386.

[42] F. J. M. Rutten, H. Tadesse and P. Licence, *Angew. Chem. Int. Ed.* **2007**, 46, 4163.

[43] R. G. Nuzzo and D. L. Allara, *J. Am. Chem. Soc.* **1983**, 105, 4481.

[44] C. A. Widrig, C. Chung and M. D. Porter, *J. Electroanal. Chem.* **1991**, 310, 335.

[45] H. O. Finklea, S. Avery, M. Lynch and T. Furtsch, *Langmuir*. **1987**, 3, 409.

[46] H. O. Finklea and D. D. Handhew, *J. Electroanal. Chem.* **1993**, 347, 327.

[47] J. Li, J. Yan, Q. Deng, G. Cheng and S. Dong, *Electrochim. Acta*. **1997**, 42, 961.

[48] H. Munakata, S. Kuwabata, Y. Ohko and H. Yoneyama, *J. Electroanal. Chem.* **2001**, 496, 29.

[49] K. Shimazu, I. Yagi, Y. Sato and K. Uosaki, *J. Electroanal. Chem.* **1994**, 372, 117.

[50] K. Sugihara, T. Teranishi, K. Shimazu and K. Uosaki, *Electrochemistry*. **1999**, 67, 1172.

[51] X. Tang, T. Schneider and D. A. Buttry, *Langmuir*. **1994**, 10, 2235.

[52] J. Wang, L. M. Frostman and M. D. Ward, *J. Phys. Chem.* **1992**, 96, 5224.

[53] K. Aoki and T. Kakiuchi, *J. Electroanal. Chem.* **1999**, 478, 101.

[54] T. Kakiuchi, M. Iida, S. Imabayashi and K. Niki, *Langmuir*. **2000**, 16, 5397.

[55] K. Bandyopadhyay, M. Sastry, V. Paul and K. Vijayamohanan, *Langmuir*. **1997**, 13, 866.

[56] H. Munakata and S. Kuwabata, *Chem. Commun.* **2001**, 1338.

[57] H. Munakata, D. Oyamatsu and S. Kuwabata, *Langmuir*. **2004**, 20, 10123.

[58] R. L. Bretz and H. D. Abruña, *J. Electroanal. Chem.* **1996**, 408, 199.

[59] M. A. Bryant and R. M. Crooks, *Langmuir*. **1993**, 9, 385.

[60] D. M. Collard and C. N. Sayre, *J. Electroanal. Chem.* **1994**, 375, 367.

[61] S. E. Creager and J. Clarke, *Langmuir*. **1994**, 10, 3675.

[62] W. R. Fawcett, *J. Electroanal. Chem.* **1994**, 378, 117.

[63] H. O. Finklea, L. Liu, M. S. Ravenscroft and S. Punturi, *J. Phys. Chem.* **1996**, 100, 18852.

[64] J. D. Green, M. T. McDermott and M. D. Porter, *J. Phys. Chem.* **1996**, 100, 13342.

[65] Z. Liu, J. Li, S. Dong and E. Wang, *Anal. Chem.* **1996**, 68, 2432.

[66] R. G. Nuzzo, F. A. Fusco and D. L. Allara, *J. Am. Chem. Soc.* **1987**, 109, 2358.

[67] T. Ohtsuka, Y. Sato and K. Uosaki, *Langmuir*. **1994**, 10, 3658.

[68] J. Redepenning and J. M. Flood, *Langmuir*. **1996**, 12, 508.

[69] E. Sabatani and I. Rubinstein, *J. Phys. Chem.* **1987**, 91, 6663.

[70] E. Sabatani, I. Rubinstein, R. Maoz and J. Sagiv, *J. Electroanal. Chem.* **1987**, 219, 365.

[71] K. Shimazu, T. Teranishi, K. Sugihara and K. Uosaki, *Chem. Lett.* **1998**, 669.

[72] K. Sugihara, K. Shimazu and K. Uosaki, *Langmuir*. **2000**, 16, 7101.

[73] D. V. Vezenov, A. Noy, L. F. Rozsnyai and C. M. Lieber, *J. Am. Chem. Soc.* **1997**, 119, 2006.

[74] M. L. Wallwork, D. A. Smith, J. Zhang, K. Kirkham and C. Robinson, *Langmuir*. **2001**, 17, 1126.

[75] M. R. Ali, A. Nishikata and T. Tsuru, *Electrochim. Acta*. **1997**, 42, 2347.

[76] J. S. Wilkes, J. A. Levisky, R. A. Wilson and C. L. Hussey, *Inorg. Chem.* **1982**, 21, 1263.

[77] T. P. Moffat, *J. Electrochem. Soc.* **1994**, 141, L115.

[78] T. Tsuda, C. L. Hussey and G. R. Stafford, *J. Electrochem. Soc.* **2004**, 151, C379.

[79] T. Tsuda, C. L. Hussey and G. R. Stafford, *J. Electrochem. Soc.* **2005**, 152, C620.

[80] T. Tsuda, C. L. Hussey, G. R. Stafford and J. E. Bonevich, *J. Electrochem. Soc.* **2003**, 150, C234.

[81] T. Tsuda, C. L. Hussey, G. R. Stafford and O. Kongstein, *J. Electrochem. Soc.* **2004**, 151, C447.

[82] G. S. Frankel, M. A. Russak, C. V. Jahnes, M. Mirzamaani and V. A. Brusic, *J. Electrochem. Soc.* **1989**, 136, 1243.

[83] G. S. Frankel, R. C. Newman, C. V. Jahnes and M. A. Russak, *J. Electrochem. Soc.* **1993**, 140, 2192.

[84] S. I. Nikitenko and P. Moisy, *Inorg. Chem.* **2006**, 45, 1235.

[85] A. Saheb, J. Janata and M. Josowicz, *Electroanal.* **2006**, 18, 405.

[86] G. A. Snook, A. S. Best, A. G. Pandolfo and A. F. Hollenkamp, *Electrohem. Commun.* **2006**, 8, 1405.

[87] M.-O. Sornein, C. Cannes, C. L. Naour, G. Lagarde, E. Simoni and J.-C. Berthet, *Inorg. Chem.* **2006**, 45, 10419.

[88] J. F. Rodriguez, T. Mebrahtu and M. P. Soriaga, *J. Electroanal. Chem.* **1987**, 233, 283.

[89] K. Aoki and T. Kakiuchi, *J. Electroanal. Chem.* **1998**, 452, 187.

[90] T. Kakiuchi, H. Usui, D. Hobara and M. Yamamoto, *Langmuir*. **2002**, 18, 5231.

[91] C.-J. Zhong and M. D. Porter, *J. Electroanal. Chem.* **1997**, 425, 147.

[92] G. R. Stafford and C. L. Hussey, *in Advances in Electrochemical Science and Engineering,* Vol. 7, R. C. Alkire and D. M. Kolb (Eds.), pp.275-347. **2001**.

[93] J. Bynestad, S. V. Winbush, H. L. Yakel and G. P. Smith, *Inorg. Nucl. Chem. Lett.* **1970**, 6, 889.

[94] Q. Liao, W. R. Pilner, G. Stewart, C. L. Hussey and G. R. Stafford, *J. Electrochem. Soc.* **1997**, 144, 936.

[95] M. Hansen and K. Anderko, *Constitution of Binary Alloys,* McGraw-Hill, New York. **1958**.

[96] S. Tamilselvi, V. Raman and N. Rajendran, *Electrochim. Acta*. **2006**, 52, 839.

[97] B. Qi, W. Lu and B. R. Mattes, *J. Phys. Chem. B*. **2004**, 108, 6222.

[98] W. Lu, E. Smela, P. Adams, G. Zuccarello and B. R. Mattes, *Chem. Mater.* **2004**, 16, 1615.

[99] L. Lizarraga, E. M. Andrade and F. V. Molina, *J. Electroanal. Chem.* **2004**, 561, 127.

[100] E. Smela, W. Lu and B. R. Mattes, *Synth. Met.* **2005**, 151, 25.

[101] R. H. Baughman, *Synth. Met.* **1996**, 78, 339.

[102] G. Han and G. Shi, *Sens. Actuators B*. **2004**, 99, 525.

[103] G. Han and G. Shi, *J. Electroanal. Chem.* **2004**, 569, 169.

[104] S. Hara, T. Zama, W. Takashima and K. Kaneto, *J. Mater. Chem.* **2004**, 14, 1516.

[105] R. A. Hillman, I. Efimov and K. S. Ryder, *J. Am. Chem. Soc.* **2005**, 127, 16611.

[106] G. Alici, B. Mui and C. Cook, *Sens. Actuators A.* **2006**, 126, 396.

[107] P. Metz, G. Alici and G. M. Spinks, *Sens. Actuators A.* **2006**, 130-131, 1.

[108] M. Koinuma and K. Uosaki, *Surface Science*. **1996**, 357-358, 565.

[109] T. P. Moffat, *Scanning Tunneling Microscopy Studies of Metal Electrodes, in: A. J. Bard and I. Rubinstein (Eds.), Electroanal. Chem., Marcel Dekker, Inc., 21 pp211-316.* **1999**.

[110] F. A. Möller, J. Kintrup, A. Lachenwitzer, O. M. Magnussen and R. J. Behn, *Phys. Rev. B.* **1997**, 56, 12506.

[111] J. Nie, H. Kobayashi and T. Sonoda, *Catalysis Today*. **1997**, 36, 81.

[112] C. Fu, H. Zhou, W. Peng, J. Chen and Y. Kuang, *Electrochem. Commun.* **2008**, 10, 806.

[113] C.-C. Tai, F.-Y. Su and I.-W. Sun, *Electrochim. Acta*. **2005**, 50, 5504.

[114] R. Bomparola, S. Caporali, A. Lavacchi and U. Bardi, *Surf. Coat. Technol.* **2007**, 201, 9485.

[115] S. Kaniyankandy, J. Nuwad, C. Thinaharan, G. K. Dey and C. G. S. Pillai, *Nanotechnology*. **2007**, 18, 125610.

[116] B. R. Panda, P. N. Rao, A. Paul and A. Chattopadhyay, *J. Phys. Chem. B.* **2006**, 110, 22917.